PHOTOEMF IN CADMIUM SULFIDE

by

K. W. Böer
Principal Investigator
Physics Department
University of Delaware
Newark, Delaware

FINAL REPORT

December 31, 1971

Prepared under Grant No. NGR 08-001-028

for

National Aeronautics and Space Administration
Lewis Research Center
Cleveland, Ohio

PHOTOEMF IN CADMIUM SULFIDE

By K. W. Böer
Physics Department, University of Delaware, Newark, Delaware

1. SUMMARY

Theoretical and experimental investigations on CdS single crystals and Cu_xS:CdS photovoltaic cells prepared from CdS single crystals by a chemical-dip procedure are described. The studies are aimed at clarifying cell mechanisms which affect key cell properties (efficiency, reliability, and lifetime) by examining the properties of intrinsic and extrinsic defects in the junction and surface regions and their effects on carrier transport through these regions.

The experimental research described includes studies of thermal, infrared, and field quenching of acceptor-doped CdS crystals; investigation of optical and electrical properties of Cu_xS:CdS photovoltaic cells (current-voltage characteristics, spectral distribution of photocurrent and photovoltage) and the dependence of these properties on temperature and light intensity; measurement of changes, as a result of heat treatment in ultra-high vacuum, in the spectral distribution of photoconductivity at room temperature and liquid nitrogen temperature, the luminescence spectrum at liquid nitrogen temperature, and the thermally stimulated current curves of CdS crystals; determination of the effect of irradiation with 150 keV (maximum) X-rays on the spectral distribution of photoconductivity and thermally-stimulated current of CdS crystals; and studies of the effect of growth conditions on the photoconductive properties of CdS crystals.

The following conclusions are arrived at: 1) A comprehensive unified model for the Cu_xS:CdS cell behavior has been developed which retains the successful features of previous major models and accounts for previously unexplained results. The model considers in detail the effects of electron traps in the CdS, recombination centers at the Cu_xS:CdS interface, and acceptor levels in the CdS on the photoelectronic behavior of the cell. 2) It is suggested that the unusually high open-circuit voltage ($\approx$ 1.0 Volt) previously observed on some Cu_xS:CdS cells is due to the fact that the Cu_xS layer is composed of djurleite ($Cu_{1.93}S$). 3) A model to explain the effects of an initial heat treatment on the performance of Cu_xS:CdS solar cells is proposed. 4) The properties of acceptor levels in CdS which are responsible for photocurrent quenching have been further clarified. 5) The dip in spectral response of a Cu_xS:CdS cell for incident light energy near the band edge of CdS is related to a trap-controlled mechanism in the CdS. 6) In order that cells be stable with respect to oxygen ambient the surface-near region of the CdS should be less Cd-rich than the bulk. 7) The conditions under which CdS crystals with different photoelectronic properties are grown have been determined with respect to ambient atmosphere and temperature during cooldown.

2. INTRODUCTION

The use of the Cu_xS:CdS photovoltaic cell to generate electricity from sunlight is interesting for several reasons:

a. Large area arrays can be inexpensively fabricated on flexible, light-weight substrates.

b. Radiation damage causes the conversion efficiency to decrease only slightly and the annealing temperatures are close to room temperature.

c. The spectral sensitivity is closely matched to the solar spectrum. Thus relatively high efficiencies are possible.

However, at present there are disadvantages which prevent large scale use of CdS solar cells. Key properties which need improvement are efficiency, reliability, and lifetime.

Unfortunately, the basic mechanisms affecting the above properties are inadequately understood. These mechanisms are related to defects in the junction and surface regions of the cell and the effect of the defects on carrier transport through these regions. It is important to understand the properties of these defects, how they are introduced into the cell, and the effects they have on cell performance in conjunction with heat treatment, illumination, interaction with ambient atmospheres, and radiation damage. Only after such knowledge is obtained can systematic development programs be carried out to enhance cell performance.

In order to most advantageously improve our understanding of the above-mentioned phenomena, the work of this research program was divided into three main categories, each building on results of previous work by this research group: The first group (J. Phillips, P. Massicot, and the Principal Investigator) has carried out extensive theoretical investigations aimed at integrating the results of current and previous experimental studies into models to explain basic cell behavior. The second group (L. van den Berg, H. Hadley, and J. Phillips) has been concerned with preparing and doping the CdS crystals, forming the Cu_xS:CdS heterojunctions, and measuring their optical and electrical properties (thermal, infrared, and field quenching; current-voltage characteristics; spectral distribution of photocurrent and photovoltage) and the dependence of these properties on temperature and light intensity. The third group (W. Devaney, J. Bragagnolo, and G. Storti) has studied the influence of radiation damage and exposure to ambient atmosphere and heat treatment on the photoelectronic properties of CdS.

3. ABBREVIATIONS

HFD	High Field Domains
IR	Infrared
I-V	Current-Voltage
LNT	Liquid Nitrogen Temperature
LS	Luminescence Spectrum
RT	Room Temperature
SDP	Spectral Distribution of Photoconductivity
TSC	Thermally Stimulated Current
TSD	Thermally Stimulated Desorption
UHV	Ultra-high Vacuum

4. TECHNICAL DISCUSSION

4.1 Extrinsic Defects in CdS Which Contribute to Photocurrent Quenching

For a detailed study of the photovoltaic effect in heterojunctions, a knowledge of the defect structure (especially for minority carriers) in the depletion region of the junction is essential, as will be discussed further in the next Section. In the case of Cu_xS:CdS heterojunctions, almost the entire depletion region occurs on the CdS side of the junction, due to the fact that the majority-carrier concentration is much larger in the Cu_xS than in the CdS. Therefore the study of defect levels in the depletion region reduces to a study of defect levels in photoconducting CdS, whose properties are similar to those of the CdS occurring in the depletion region of Cu_xS:CdS photovoltaic cells. The CdS side should be similar to CdS doped with copper (CdS:Cu), since Cu diffuses into the CdS during the standard heat treatments given these cells. A study of CdS:Ag was undertaken to investigate defect structure for minority carriers in a similar system (Ag doping was used because of ease of preparation and its similarity to Cu doping).

The defect structure for minority carriers can best be studied by quenching effects which redistribute minority carriers among levels in the band gap and thus change the majority carrier lifetime. There are three main ways that this quenching may be initiated: First, by thermally redistributing holes from trapping or slower recombination centers to faster recombination centers (thermal quenching (ref. 1)); second, by redistributing the holes by optical excitation (ref. 1) (infrared (IR) quenching); finally, by redistribution of holes from slow to fast recombination centers by changing trapping parameters using high electric fields (field quenching (refs. 2 and 3)).

In order to investigate the quenching effects, the doping of crystals for reproducibility and high sensitivity to quenching had to be accomplished. CdS crystals were grown using a vapor transport process at atmospheric pressure, in which a carrier gas stream (N_2; 0-5 vol. % H_2S) transports evaporated CdS powder from a hot region in the growth furnace to a cooler region where crystallization takes place. The growth conditions are determined by varying the % of H_2S in the carrier gas and the temperature gradient in the crystallization region. The temperature at which the H_2S is turned off during cooldown can also significantly affect the photoelectronic properties of the CdS platelets, and studies along these lines are described in Section 4.7 below. In a separate process the crystals were doped with differing amounts of Ag and compensated with Al to produce high sensitivity to all three types of quenching.

To test the reproducibility of the doping procedure, various crystals were investigated using the technique of high field domains (HFD) to study the field quenching (refs. 4 and 5). It was found that a concentration of

50 parts per million (ppm) Ag produced crystals with the most sensitivity to field quenching with reproducible results (using the doping procedure described in ref. 6). Crystals thus prepared showed quenching over 2-3 orders of magnitude, rather than the usual few percent, and the results were very reproducible (ref. 6).

Figure 4.1.1 shows the typical behavior of thermal quenching for these crystals. Notice that there are two quenching regions, one around -40° C where the electron concentration (n) decreases by roughly a factor of 2, and the second, above 60° C, where n drops by 2 orders of magnitude. In the intermediate regions the lifetime is approximately constant with changes in temperature, though the values are different. Region 2 has an activation energy of 0.9 electron Volts (eV). Region 1 was not reproducible enough to give an activation energy.

Figure 4.1.2 gives the photocurrent response as a function of IR bias light showing the well known optical quenching spectrum. The two curves are for temperatures above and below region 1 of the thermal quenching curve (Figure 4.1.1). The two quenching peaks (λ (wavelength) = 900 mμ (millimicrons) and λ = 1.37 μ) correspond to optical transitions of 1.4 eV and 0.9 eV. The 0.9 eV peak disappears at temperatures below -40° C.

Figure 4.1.3 shows the field quenching behavior as revealed by HFD analysis. Notice that for electric fields below about 20 kiloVolts per centimeter (kV/cm) field quenching is masked and then decreases n by roughly 3 orders of magnitude above this critical field.

These three types of quenching can all be explained, at least qualitatively, by means of a model containing a number of different centers for recombination that have different recombination coefficients (fast and slow recombination centers). In order to obtain more detailed information (e.g. on energy levels, trapping parameters, etc.) the effects of simultaneous quenching by different means were studied.

Since the quenching data suggest 2 levels for hole storage, the thermal emptying of these levels in combination with IR emptying was investigated. Figure 4.1.4 shows the thermal quenching with IR bias light (to partially empty one of the levels). It is interesting to notice the behavior in quenching region 1. In this region, with 0.9 eV bias light, major quenching occurs with an activation energy of 0.50 eV. 1.4 eV bias light alone causes quenching throughout the whole temperature range, showing a tendency to duplicate region 1's thermal quenching.

The effect of thermal and/or IR quenching on field quenching is to unmask the field quenching at lower field strengths. Figure 4.1.5a shows the effect of thermal quenching on field quenching, and Figure 4.1.5b shows the effect of IR quenching (λ = 950 mμ). It might be noted that the IR unmasking of field quenching has the same spectral response as the IR quenching of photoconductivity (Figure 4.1.2).

Since IR and thermal quenching both influence the field quenching in the same way, this implies that the same centers are involved and that the effects of all three types of quenching complement each other. From the 0.5 eV thermal activation of quenching with 0.9 eV bias light, it appears that the two levels involved in the infrared quenching are "connected"; i.e. direct thermal exchange between these two levels occurs. Burgett and Lin (ref. 7) have studied IR quenching of photoconductivity and Hall coefficient and noted this 0.5 eV transition optically in CdS:Cu, thus providing further evidence of the similarity to CdS:Ag.

The defect level structure for minority carriers can thus be described best by three levels as indicated in Figure 4.1.6 where the H and S centers are connected (transitions "a" and "b"). The different recombination coefficients cause recombination rates to vary when recombination occurs through different channels. Majority carrier lifetime is shortest when recombination through F centers predominates and longest when recombination through S centers is the dominant channel. The effect of increasing temperature is first to cause a redistribution of holes from S to H centers, changing the lifetime approximately by a factor of 2 (thermal quenching region 1), and then to empty the holes from both centers via a two-step process (from S to H to the valence band) so that they may recombine at F lowering the lifetime by several orders of magnitude.

The role of the IR quenching is not as straightforward. The 1.4 eV light must empty holes from the S centers, but the 0.9 eV transition may be either "a" or α_H (Figure 4.1.6). Thus the energetic distance from the valence band to the S centers should be ~1.4 eV and the H centers may lie either 0.5eV (refs. 8 and 1) or 0.9 eV above the valence band. The red response in the photoconductivity noted in these crystals with a threshold of 1.5 eV (ref. 1) implies that the H centers should be placed 0.9 eV from the valence band edge. The 0.9 eV bias light then acts to increase transition α_H and the 1.5 eV light excites H center electrons to the conduction band.

At temperatures below those of region 1 (Figure 4.1.1) the 0.9 eV light has little effect, implying that at these temperatures not enough holes are stored in the H centers to make the fast recombination (through F, due to holes excited into the valence band by the 0.9 eV light and then trapped at F centers) comparable to the slow (through S) . Above -40° C, holes may be shifted thermally from S to H and by a 0.9 eV optical transition, shifted to the valence band and thence trapped at F. Thus quenching may occur. The duplication of the thermal quenching by 1.4 eV bias light is explained if the α_S transition is not increased enough to completely dominate the thermal release path (S to H to the valence band to F).

Field quenching is unmasked by thermal and IR quenching because the field no longer has to do all the shifting of recombination. Therefore the quenching, which occurs when F center recombination traffic is comparable to the S-H center traffic, occurs at lower field strengths.

The most likely defect structure thus has three main levels, S, H and F. S levels lie 1.4 eV above the valence band, while H levels lie 0.9 eV above the valence band. Both can act as recombination centers under suitable conditions, the resulting majority carrier lifetimes differing by about a factor of 2. F levels, probably lying above the S centers, give rise to a lifetime approximately 2 orders of magnitude shorter than that of the slower centers. The defect levels discussed in this Section will be incorporated in a unified band model of the Cu_xS:CdS photovoltaic cell in the following Section.

4.2 A Unified Band Model for the Cu_xS:CdS Photovoltaic Cell Produced by the Chemical Dip Method

There have been two major band models proposed for the Cu_xS:CdS photovoltaic cell. The first was proposed by Shiozawa et al. (ref. 9) of the Clevite Corporation and will be referred to as the Clevite model (see Figure 4.2.1). The second was put forth by Bube et al. (refs. 10 and 11), of Stanford and will be called the Stanford model (see Figure 4.2.2). The Stanford model was proposed to explain experimental data which seemed to be in contradiction with the Clevite model. This discussion will try to show how a unified band model can explain both sets of data.

Figure 4.2.3 shows the band model for the cell before any type of heat treatment. It is shown with the conductivity $\sigma \approx 1$ ohm (Ω) -cm for n-type CdS ($E_C - E_F \approx 0.2$ eV, where E_C is the conduction band edge and E_F is the Fermi level) and almost degenerate p-type Cu_xS ($E_F - E_V \lesssim 0.02$ eV, where E_V is the valence band edge). Also included are states at the interface which can act as recombination centers.

The difference in energy between the conduction bands of Cu_xS and CdS at the interface, ΔE_c, is picured as being 0.35 eV. This implies that a response due to photo-emission of electrons from the Cu_xS valence band into the CdS should occur for incident photon energies ≥ 0.85 eV (see insert in Figure 4.2.3), and such a response has been observed (ref. 12). Furthermore, the maximum observed open circuit voltage (V_{oc}) of 0.85 Volts (ref. 9) can be explained by such a ΔE_c, as is shown in Figure 4.2.4. Under high illumination intensities, the electron quasi-Fermi level in the CdS could approach the conduction band (Figure 4.2.4a). If the open circuit voltage increased above 0.85 eV (Figure 4.2.4b), conduction electrons in the CdS would drift towards the interface, and if extensive recombination could occur at the interface, such a further increase in V_{oc} would be counteracted, as is found experimentally.

Under forward bias conditions a forward barrier height of 0.65 Volts would be expected if recombination dominated and a forward barrier height of 1 Volt if there were no interface recombination current (see Figure 4.2.5). Ordinarily a forward barrier height between these two extremes would be measured, which is the case (ref. 13).

Tunneling currents observed under low forward bias (see ref. 13, p. p. 173) can be explained by electron traps in the CdS between 0.2 and 0.65 eV below the conduction band. Near the interface these would be ionized, leaving a higher positive charge than in the rest of the space charge region. This would narrow the conduction band "wedge" in this region and allow tunneling to the interface states (see Figure 4.2.6). In addition, this would cause an increase in recombination when V_{oc} under illumination reached this tunneling voltage and change the slope of the V_{oc} vs. illumination intensity (ref. 13, pp. 98-101).

The recombination at the interface states will also appear in the I-V characteristics of the cell under illumination as a shunt resistance. This will give the cell a high dI/dV near the short-circuit current (I_{sc}) leading to a poor "fill factor". A slight heat treatment could anneal out some of the interface states and improve this characteristic.

Also, the heat treatment will cause Cu to be incorporated into the CdS creating the sensitizing levels H and S in the CdS which trap electrons and widen the space charge layer (see Figure 4.2.7). A slight incorporation of Cu will widen the space charge layer sufficiently to eliminate tunneling and hence improve V_{oc} as is commonly found.

Further heat treatment will incorporate more Cu in the CdS and create a layer of "compensated" CdS adjacent to the Cu_xS:CdS junction much like that proposed in the Clevite model. Because most of the junction is in the CdS away from the Cu_xS:CdS interface, the photovoltaic response from the Cu_xS will be reduced since photogenerated electrons diffusing from the Cu_xS to the CdS can recombine in the compensated CdS before they reach the electrical junction between the i-CdS and the n-CdS. If the response is reduced as described above, there may be a rise in response at 1.8 eV due to another conduction band minimum of Cu_xS at this energy (see Figure 4.2.7). This rise would occur due to the following: First, the electrons coming from the Cu_xS would be injected into the CdS approximately 1 eV above the CdS conduction band edge. Consequently, before the electrons thermalized to the conduction band edge and thence were killed at recombination centers, they would have to undergo many collisions with phonons as they diffused through the CdS. During this diffusion process many electrons could reach the electrical junction in the CdS and contribute to the response before they recombined. This may account for the observation by several investigators (refs. 11 and 14) of 1.8 eV thresholds in the spectral response of Cu_xS:CdS photovoltaic cells.

The enhancement and quenching of the photovoltaic effect can be explained with the unified model in a manner similar to that of the Stanford model except for a different energy level scheme (see the previous Section). Light of energy $\geq$ 1.5 eV can excite electrons from the H levels to the conduction band where they drift out, thereby changing the junction to the non-heat treated case. Band to band excitation in the CdS ($h\nu \geq 2.4$ eV, where h = Planck's constant and ν is the frequency of the light) will do the same thing since when an electron-hole pair is excited by the band to band light, the hole will be trapped at an H or S level and the electron will drift out of

the space charge region. A hole trapped at an H level can then be excited to an S level, since the two types of levels are thermally connected (see Section 4.1). Illumination with light of energy $h\nu$ = 0.9 eV or 1.4 eV will put electrons back in the H level and "quench" the response. Electrons coming from the Cu_xS can also be slowly trapped by these levels, thereby also quenching the response.

Enough Cu can be incorporated into the CdS so that the intensity of light reaching the CdS is not sufficient to restore the original junction and hence the photovoltaic response remains degraded. It can, however, be restored by thermal means. Heating for a sufficient amount of time will also excite electrons from H thermally (much like thermal quenching of photoconductivity) and restore the original junction. Optical excitation of the Cu_xS will slowly allow electrons to fill these levels again and "optically degrade" the junction back again.

Much of what has been discussed can also be explained similarly with the Stanford model. The data that do not seem to be able to be reconciled with the Stanford model, and which can be explained by the unified model proposed here are:

1. The longwavelength photoresponse to 0.85 eV.

2. The maximum measured V_{oc} of 0.85 Volts.

3. The onset of forward bias tunneling at voltages of 0.2 V (see ref. 13, p. 173). (One would expect it to occur near 1 V in the Stanford model.)

4. The increase in response at 1.8 eV after heat treatment.

5. A forward barrier height as low as 0.65 eV.

There is one further thing to note. The decrease in slope of the V_{oc} curves vs. illumination intensity at $V_{oc} \approx 0.45$ Volts, mentioned above, can also be explained by a level in the Cu_xS band gap $\approx$ 0.45 eV above the valence band. This level could "pin" the electron quasi-Fermi level here until it was filled. There is evidence for this level, probably due to excess Cu, in Hall effect measurements and light absorption data (ref. 15).

More work is being done to put these ideas into more specific form along with work based on P. N. Keating's paper (ref. 16) to semiquantitatively predict the electrical characteristics of the junction.

4.3 Experimental Study of the Structure in the Spectral Response of Cu_xS:CdS Photovoltaic Cells for $h\nu \approx 2.4$ eV

In a previous report (ref. 6), experiments were done to examine the dip in the response of I_{sc} and V_{oc} vs. λ near the band edge of CdS, ≈ 2.4 eV. Further experiments have been performed to examine this spectral dip on Cu_xS:CdS heterojunctions made from CdS platelets, grown as described in Section 4.1, by a chemical-dip technique. The chemiplating procedure by which the Cu_xS was formed on the CdS crystals was performed as follows: An aqueous solution of CuCl was prepared by first dissolving $CuCl_2$ in concentrated HCl with excess Cu. This was boiled until the liquid turned clear. Then cold H_2O was added to precipitate out the CuCl. The CuCl was rinsed three or four times with cold water before using.

Prior to the chemiplating dip, the CdS crystal ($\approx$ 1 mm x 2 mm x 0.1 mm) was placed on a glass slide and encapsulated in an epoxy (Sylgard 51 Dielectric Gel made by the Dow Corning Co.) which was cured at 75° C for 3/4 to two hours. Then the surface of the crystal on which the Cu_xS was to be chemiplated was exposed by cutting away the epoxy with a razor blade. Following this the glass slide and the CdS crystal were dipped in a 25% solution of HCl for about a minute to etch slightly the exposed surface of the CdS.

After this the chemiplating dip was performed. This consisted of placing the slide with the crystal in a saturated aqueous solution of CuCl kept at 90° C for 1/4 to 1-1/2 hours. This formed a Cu_xS layer 10 to 50 microns thick on the exposed surface of the CdS crystal.

The crystal was then removed from the epoxy. Either before or after the Cu_xS layer was formed, an ohmic Ti;Al contact was evaporated onto the CdS. Electrical contact was made to the Cu_xS and Ti/Al by cementing on Cu wires with silver print.

It should be noted that after the formation of the Cu_xS layer, no heat treatments were performed; and all further measurements were made with the crystals in an N_2 atmosphere.

The Cu_xS junction and the Ti/Al contact were put on these platelets on the large face parallel to the C-axis (see Figure 4.3.1). After the Cu_xS layer was on these crystals, the edges perpendicular to the layer and parallel to the C-axis were cleaved off to remove any possible Cu_xS on these edges that might have diffused under the epoxy. In this way illumination could be incident on the Cu_xS layer first (frontwall cell) or the CdS first (backwall cell).

A double monochromator arrangement was used to enable the simultaneous illumination of the cell with light of two different wavelengths as shown in Figure 4.3.1. For the spectral measurements one light source was kept at a constant wavelength (bias light) while the wavelength of the second was varied.

Figure 4.3.2 shows the spectral response of I_{sc} vs. λ for a single source. The spectral dip occurs at $\approx$ 0.515 μ. Figure 4.3.3 shows the spectral response of I_{sc} for various bias wavelengths (λ_1). From this it can be seen that illuminating the cell with light at the spectral dip decreases the cell response.

In order to determine if this spectral dip is associated with absorption occurring in the CdS, V_{oc} vs. λ was measured with low intensity polarized light. Figure 4.3.4 shows the results with the bias light at λ_1 = 0.6 μ (unpolarized) in order to increase the sharpness of the dip. The polarization response follows that of CdS (ref. 17) clearly indicating that the phenomenon causing the spectral dip is related to absorption in CdS.

Further time response measurements were done on V_{oc} to investigate the possibility that the dip in response is trap controlled and connected with the junction area. Figure 4.3.5 shows V_{oc} vs. time with the Cu_xS shadowed from the 0.515 μ light (only the CdS and the junction are illuminated (see ref. 6)). The 0.6 μ source illuminates the entire cell. We can compare this to Figure 4.3.6 where both sources illuminate the entire cell. In both cases the long recovery time of the 0.6 μ light after the 0.515 μ light is switched off ($t > t_7$) indicates that the process is trap controlled. Furthermore, it should be noted that the 0.515 μ light has two effects. First of all, by itself it causes a positive photoresponse, as can be seen in the time segment $t_5 - t_6$. Secondly, it causes a large decrease in the response to the 0.6 μ light. It is suggested that the positive response arises mainly from the 0.515 μ light which is absorbed in the Cu_xS, while the reduction in the 0.6 μ is caused by 0.515 μ light absorbed in the CdS which prevents electrons excited in the Cu_xS from reaching the electrical junction in the CdS. The sharp decrease in response at time t_7 in Figure 4.3.6 when the 0.515 μ light is turned off is due to the removal of the positive response while the trap-controlled blocking mechanism has not yet decayed.

4.4 Further Discussion of the Interlayer Model for Cu_xS:CdS Photovoltaic Cells

In a previous report (ref. 6) a model was proposed for the Cu_xS:CdS photovoltaic cell which accounted for several previously unexplained experimental results. The main feature of the model is an interlayer of djurleite ($Cu_{1.93}S$) which can be created and dissipated at a Cu_2S:CdS heterojunction by a thermal and a photochemical process, respectively. Two applications of the model will be discussed below: First, the possibility that the unexplained high V_{oc} observed by Chamberlin (refs. 18 and 19) and co-workers on Cu_xS:CdS photovoltaic cells is due to a $Cu_{1.93}S$:CdS heterojunction and second, an explanation of the heat treatment which is necessary for good solar cell performance.

In the process of studying Cu_xS:CdS photovoltaic cells made by the chemical-spraying technique, Chamberlin and co-workers obtained cells with an unexplained V_{oc}, up to $\approx$ 1.0 eV (refs. 18 and 19). It is suggested here that these cells have a Cu_xS-layer which consists essentially of djurleite. This is supported mainly by two observations. 1.) The room-temperature spectral response of the high-voltage cells has a threshold at $\approx$ 1.8 eV (ref. 20), indicating that the composition of the Cu_xS possibly is mainly djurleite, based on the assumption of the interlayer model that the band gap of djurleite is 1.8 eV (ref. 6). 2.) The increase in V_{oc} is about what one would expect as a result of the cell being composed of $Cu_{1.93}S$:CdS as opposed to Cu_2S:CdS. This can be seen from the following plausibility argument: First, one can assume that the electron and hole lifetimes in the bulk CdS are independent of the phase of copper sulphide. In addition, both Cu_2S and $Cu_{1.93}S$ are degenerate (ref. 21). This fixes the hole quasi-Fermi levels in both materials approximately at the valence band edge. If one then assumes that the electron lifetimes in the $Cu_{1.93}S$ satisfy the following approximate relationship, τ_n ($Cu_{1.93}S$) $\lesssim$ τ_n (Cu_2S), one finds that all differences between the electron and hole quasi-Fermi levels and the conduction and valence bands, respectively, are approximately the same in both types of cells. This implies that the difference in band gaps in the $Cu_{1.93}S$ and the Cu_2S is reflected in a similar difference in the separation of the electron and hole quasi-Fermi levels in the two materials under illumination. When either of the two materials is joined to CdS, this difference in quasi-Fermi level separation will lead to a corresponding difference in V_{oc} (Figure 4.4.1).* The difference in V_{oc} of the two types of cells ($\approx$ .5 V) is consistent with the difference in band gaps ($\approx$ .6 eV).

The second application of the interlayer, which will now be discussed, could have important implications for the production of solar cells. The initial heat treatment on Cu_xS:CdS solar cells is essential for good device performance. The available data are consistent with the following model:

---

* The method of constructing these energy-band diagrams is described in more detail elsewhere (ref. 6).

1. Heat treatment leads to the formation of the djurleite barrier, as described above. This leads to a reduction in I_{sc}.

2. Metallic copper, which will short out the junction (not necessarily the entire layer), can be initially deposited, along with the Cu_xS, on defective CdS surfaces. A heat treatment in vacuum will result (in addition to the previous effect) in the reaction of the copper with the CdS to form Cu_xS. A heat treatment in air will remove the shorts more quickly, due to oxidation of the copper. This effect of heat treatment increases the shunt resistance, thereby improving the photovoltaic properties.

The data on which these conclusions are based include the following:

a. Thin film cells require a heat treatment before they exhibit good photovoltaic behavior. For example, Brandhorst and the Lewis group (ref. 14) reported that before heat treatment, the thin-film cell characteristic was poor, as was evidenced by a large reverse saturation current (a result of shorting out part of the junction). Heat treatment improved the characteristic but decreased I_{sc}.

b. Most known cells which have not needed an initial heat treatment before displaying good photovoltaic performance have been single-crystal cells (refs. 11 and 22), which have less defective surfaces than thin-film cells. For example, Gill and Bube (ref. 11) reported that good cells could always be formed on carefully prepared CdS (single crystal) surfaces. A heat treatment was always detrimental to the photovoltaic properties of such cells, due to a decrease in I_{sc}. However, they observed many cells with poor current-voltage (I-V) characteristics before heat treatment. These cells generally showed improved photovoltaic properties after a short heat treatment which, they stated, could be attributed to decreased shunt losses.

c. Copper oxidizes extremely slowly in air at room temperature. When heated to above 200° C, however, it begins to oxidize rapidly to Cu_2O (ref. 23). This correlates with the empirical result that the optimum temperature for a short heat treatment in air is above 200° C.

d. Bube and his group performed experiments on cells made by electroplating copper on CdS. Although there was no visible trace of Cu_2S, the long-wavelength response was high and the spectral response was flat to ≈ 940 mμ, indicating the presence of Cu_2S at the interface with CdS. Furthermore, I_{sc} approached the value obtained with the best dipped cells, for some samples. However, all plated cells had poor diode characteristics in the light and dark, resulting in a very

low V_{oc} (ref. 24). These results indicate high shunt losses (ref. 25). This and the fact that there was apparently much more copper present than is usually the case in dipped cells support the proposed model.

The implications of the above discussion concerning device performance will now be discussed. First of all, a suggestion can be made for improving thin-film device performance: recrystallization of the CdS film before deposition of Cu_xS. Such a recrystallization (ref. 26) has been attempted. However, this previous method utilized the incorporation of silver in the CdS and led to shorting of the junction due to silver precipitation (ref. 27). This, of course, is one of the effects one wishes to prevent. A better recrystallization procedure should be employed, following, e.g., the method described by Böer et al (ref. 28). The present paper predicts that if this were successful, the need for the initial heat treatment, which degrades I_{sc}, would be alleviated. In addition, the gradual degradation of I_{sc} would be retarded, since the more stable CdS surface would be more resistant to attack by copper from the copper sulphide. Thus the formation of djurleite (and eventually other phases of copper sulphide) would be slowed.

The possibility that the high-voltage cells reported by Chamberlin et al are $Cu_{1.93}S$:CdS cells should be investigated. This would be of practical interest. If the high-voltage cells are $Cu_{1.93}S$:CdS cells, maximum-efficiency calculations (ref. 29) predict that they would probably not be able to compete with other cells, because the band gap of $Cu_{1.93}S$ is too large. On the other hand, if the high-voltage cells are discovered to be Cu_2S:CdS cells, the mechanism causing such a large V_{oc} should be determined.

It should be noted that both the interlayer model discussed in this Section and the unified model introduced in Section 4.2 provide interpretations of observed phenomena related to a spectral response threshold at $\approx$ 1.8 eV. Further data are required to determine which model provides the correct explanation or if the processes discussed in both models occur. From the standpoint of intrinsic appeal, the unified model's explanation is to be preferred because of its greater simplicity.

4.5 Effect of Heat-treatments in Ultra-high Vacuum on the Photoelectronic Properties of Undoped Class I CdS Platelets

E. F. Gross and B. V. Novikov (ref. 30) were the first to observe the correlation between absorption and spectral distribution of the photocurrent (SDP) in the exciton region at liquid nitrogen temperature (LNT). On this basis, they defined two main types of CdS crystals: Class I crystals for which the maxima in the free-exciton absorption spectrum appeared at the same energies as the maxima in the SDP, and Class II crystals, for which maxima in absorption corresponded to minima in the SDP.

This definition was later extended to include other photoelectronic properties (refs. 4, 31 and 32): At room temperature (RT) the SDP of Class I

crystals shows a shoulder for photon energies $h\nu > E_g$, where h is Planck's constant, ν is the photon frequency, and E_g is the band gap. For Class II crystals, the photocurrent drops considerably for the same energies after passing through a maximum. Also, the green-edge photoemission at LNT is intense for Class I and weak for Class II crystals.

The photoelectronic properties of Class I CdS platelets have been shown to be strongly affected by short heat-treatments in ultra-high vacuum (UHV) at temperatures below 400° C, while those of Class II crystals remain relatively unchanged. A heat treatment at about 200° C changed a Class I crystal to Class II (refs. 4, 31 and 32).

Mass spectroscopic measurements have demonstrated that heat treatments can cause significant desorption of gases from the surface of CdS (refs. 4 and 31). In particular, oxygen (atomic mass unit (AMU) 16) and Cd desorption have been detected in thermally stimulated desorption (TSD) measurements. In this case, a change in the shape of the SDP at RT, indicating a transition from a Class I to a Class II crystal, has been observed at temperatures above 400° C where Cd desorption becomes important.

This report describes the changes in the SDP at RT and LNT, the luminescence spectrum (LS) at LNT and the thermally stimulated current (TSC) curves of Class I CdS platelets, grown as described in Section 4.1, as a result of heat-treatments in UHV. In an attempt to determine the influence of the heating rate on the temperature at which the transition from Class I to Class II occurs, experiments were conducted on two halves of a cleaved CdS crystal of Class I.

Our experimental arrangement was as follows. Two similar stainless steel UHV chambers were used. The selected undoped CdS platelets with evaporated Ti-Al electrodes having slit geometry with 5 mm x 5 mm uncovered CdS were mounted in thermally shielded crystal holders within the chambers. Electrical connections with the outside of the chambers were provided and light could enter the chambers by suitable windows (for details, see ref. 6). One of the chambers (system A in what follows) was equipped for the analysis of the gases desorbed from the surface of the CdS. The temperature of the crystal was increased by Joule's heating and a linear increase in temperature up to 400° C (suitable for TSD measurements) with various heating rates (up to about 5° C/sec.) was obtained. Spectroscopic analysis was carried out with a 1m. Jarrell-Ash spectrometer, used as a monochromator for SDP and LS measurements at LNT on crystals mounted in the second chamber (system B). Heat treatments were performed in system B by heating the crystal holder at rates of up to 0.2° C/sec. For luminescence excitation, an HBO-200W-Mercury lamp with 365-nm and heat glass filters were used. The luminescence was detected using an RCA, 1P21 type phototube. The spectral slit width was about 1.6 Ångstroms (Å) for LNT and 3 Å for RT measurements.

Now we present our results. The SDP's at RT of crystals 861-1 (Figure 4.5.1) and 861-2 (Figure 4.5.2) are shown after a series of heat treatments carried out on both crystals. They were obtained by cleaving

along the c-axis a single crystal on which contacts had been previously deposited. The heating rate used for heat-treatments on crystal 861-1 (5.6° C/sec.) was about a factor of 30 higher than that used for those on crystal 861-2, (0.18° C/sec.). The behavior observed in both cases is consistent with earlier experiments. Starting with the SDP at RT for the untreated crystals (curves 4.5.1-1 and 4.5.2-2) the ratio of the intrinsic (wavelength (λ) = 460 mμ (millimicrons)) to extrinsic (λ = 518 mμ) photocurrents increased upon pumping from atmospheric pressure to 10^{-9} torr. Heat treatments up to a certain temperature do not change the Class I character of the SDP, while the initial SDP can be partially restored by oxygen backfilling. For the high heating rate (curve 4.5.1-2) a highly conducting state is reached after a treatment at 225° C, with a very low value of both the intrinsic to extrinsic photocurrent ratio and the red sensitivity (λ= 600 mμ). A treatment at 380° C increases the intrinsic to extrinsic ratio and the red sensitivity (curve 4.5.1-3) and causes the photocurrent to decrease. A transition to Class II occurs upon treatment at 400° C, (curve 4.5.1-4).

For the low heating rate, no high conductivity state is obtained previous to the transition to Class II (curves 4.5.2-2 and 4.5.2-3). This transition occurs upon treatment at 210° C (curve 4.5.2-4). Treatments at higher temperatures caused an essentially parallel displacement of the Class II SDP towards higher currents.

The effect of heat-treatments on the SDP at LNT of crystal 861-2 is shown in Figure 4.5.3 for the electric field vector (E) of the incident light parallel to the CdS c-axis. The virgin crystal showed a Class I SDP (curve 4.5.3-1). The position of the B_1 exciton (ref. 33) optical absorption is indicated by the arrow, as obtained from reflection spectra.

After a 180° C heat treatment, the spectrum is still of Class I but shows an additional peak at λ = 4910 Å, (curve 4.5.3-2). This peak is resolved into finer structure and reduced by oxygen backfilling (see ref. 6). After 240° C and 300° C treatments (curves 4.5.3-3 and 4.5.3-4) the photocurrent increased by several orders of magnitude and minima appear where maxima were previously located. Results for $E \perp c$ were consistent with the above.

The changes in the green-edge emission are shown in Figure 4.5.4, for crystal 861-2. Two treatments at 240° C and a treatment at 270° C strongly reduced the luminescence.

The TSC curves were measured for crystal 861-2 before and after each treatment, for both extrinsic and intrinsic excitation. The results of the measurements are presented in normalized form in Figure 4.5.5. The quantity plotted vertically, is

$$a \cdot \frac{I_{TSC}}{I_{ph}} \cdot \frac{1}{b}$$

where a is the excitation density, I_{TSC} is the TSC current measured, I_{ph} is the photocurrent measured under the excitation density a and b is the

heating rate. For intrinsic excitation, $a \approx 10^{17}$ photons cm^{-3} sec^{-1}. For extrinsic excitation, $a \approx 10^{14}$ photons cm^{-3} sec^{-1}. The heating rate used was $b = 0.1°$ K/sec. The trap density for a particular TSC peak between temperatures T_1 and T_2 is very roughly given by:

$$N_t \approx \int_{T_1}^{T_2} a \frac{I_{TSC}}{I_{ph}} \frac{i}{b} \cdot dT \quad .$$

Table 1 further illustrates the dependence of the treatment temperature that caused a transition from Class I to Class II on the heating rate as determined for a series of crystals.

Crystal	Transition Temperature	Heating Rate
	[°C]	[°C/sec.]
811-1	450	5.0
834	440	5.0
861-1	400	5.6
861-2	210	0.18
838-1	250	0.1

TABLE 1

The possibility of current channeling occurring as a consequence of Joule's heating, was investigated by monitoring the crystal current and the voltage across it as a function of temperature for a CdS platelet, mounted in system A. The heating rate used was 5.0° C/sec. The conductivity decreased slowly up to about 450° C and channeling occurred at about 575° C, a temperature considerably higher than the transition temperatures observed.

Now we discuss our results.* In a Class I CdS crystal the surface near layer differs from the bulk in that it contains a higher concentration of excess Cd yielding a donor concentration of about $N_t \approx 10^{18}$ cm^{-3} (ref. 31). (This can also be seen from Figure 4.5.5, where the trap density obtained in the surface near region (intrinsic excitation) is three orders of magnitude above that in the bulk (extrinsic excitation)).

* As a general reference for the following discussion, consult ref. 1.

Quantitative TSD measurements show that a heat treatment can desorb a surface density $\Sigma_s \approx 10^{15}$ cm^{-2} oxygen atoms from the surface of a Class I CdS crystal. When at the surface, a maximum determined by the breakdown field $F_B \approx 10^6$ V/cm of about:

$$\Sigma_M = \frac{\varepsilon\varepsilon_o}{e} F_B \approx 10^{13} \text{ oxygen atoms/cm}^2 ,$$

(where ε is the dielectric constant, ε_o is the permitivity of free space, and e is the electronic charge), are filled with electrons coming from the donors in the surface near region. The resulting negative charge is compensated by the positive charge of ionized donors in a region of width:

$$\Delta = \frac{\Sigma_M}{N_t} \approx 10^{-5} \text{ cm} .$$

When strongly absorbed excitation is used on a CdS platelet,* having a thickness $d \approx 10^{-2}$ cm, light is absorbed in a region of thickness

$$\delta_1 \approx \frac{1}{k_i}$$

($k_i \approx 10^5$ cm^{-1} is the intrinsic absorption constant) where it creates electron hole pairs and excitons. Electron-hole pairs diffuse until the holes are trapped, through a distance $\delta_2 \approx \Lambda_a$, the ambipolar random-walk length. It has been shown that when $\mu_n\tau_n >> \mu_p\tau_p$ ($\mu_{n,p}$ and $\tau_{n,p}$ are the mobilities and lifetimes of electrons and holes respectively) then $\Lambda_a = \sqrt{2}\ \Lambda_p$, where Λ_p is the hole random-walk length (ref. 34). We have:

$$\Lambda_p = \sqrt{v\ \tau_p\lambda_p}$$

where v is the hole thermal velocity and λ_p is the hole mean free path, as can be seen from the following argument: The random-walk length Λ_p is the net displacement of the hole from birth to death. This distance, by random-walk theory, is the mean free path times the square root of the number of collisions with phonons (i.e., the number of random steps), N_{coll}:

$$\Lambda_p = \lambda_p \sqrt{N_{coll}}$$

But N_{coll} is the lifetime divided by the time between collisions, $\tau_c = \lambda_{p/v}$:

$$N_{coll} = \frac{\tau_p}{\tau_c} = \frac{\tau_p}{\lambda_{p/v}} = \frac{v\tau_p}{\lambda_p} .$$

Thus

$$\Lambda_p = \lambda_p\sqrt{\frac{v\tau_p}{\lambda_p}} = \sqrt{v\tau_p\lambda_p} .$$

---

* See Figure 4.5.6.

We also have:

$$\tau_p = \frac{1}{v N_r \sigma_p} \qquad \text{(ref. 1)}$$

where N_r is the density of recombination centers and σ_p is the hole capture cross section. Accordingly $\delta_2 < 10^{-5}$ cm for reasonable values of $\lambda_p \simeq 100$ Å, $N_r \simeq 10^{17}$ cm^{-3} and $\tau_p > 10^{-13}$ cm^{-2}.

Once holes are trapped, electrons diffuse through a distance $\delta_3 \sim L_D$, the Debye length. For trap dominated photoconductivity, as in our case (ref. 35):

$$L_D = \sqrt{\frac{\varepsilon\varepsilon_o \, kT}{e^2 N_t}} < 10^{-5} \text{ cm for } N_t > 10^{15} \text{ cm}^{-3},$$

where k is Boltzmann's constant and T is the absolute temperature. Excitons diffuse before dissociating into electron-hole pairs, through a distance $\Lambda_e < \Lambda_p$ where Λ_e is the exciton random walk length (ref. 36). Therefore, electron-hole pairs are not produced beyond a distance Λ_p from the surface. The region where photoconductivity occurs, then has a width:

$$\delta = \delta_1 + \delta_2 + \delta_3 \simeq \frac{1}{k_i} \simeq 10^{-5} \text{ cm} \quad .$$

This region has the same size as the space charge region of width Δ whose properties depend very strongly on the surface adsorbed oxygen. As oxygen desorption proceeds, electrons are released by the outgoing oxygen into the donors in this space charge layer. As a consequence of the excess Cd a strong accumulation layer remains. The electron lifetime

$$\tau_n = \frac{1}{v \sigma_n h_r}$$

(where v is the thermal velocity of the electrons, σ_n is the capture cross section for electrons and h_r is the density of recombination centers containing holes), increases towards the surface since h_r is then depleted. In the high absorption region of the spectrum, the photocurrent

$$i = \frac{eN}{t_d} \tau_n$$

(where N is the excitation rate and t_d the drift time) is proportional to τ_n, since N and t_d do not depend on the excitation wavelength. As the optical absorption increases in the exciton peaks, the photoelectrons are confined to a region of diminishing width

$$\delta \simeq \frac{1}{k_i} \quad ,$$

experiencing a higher lifetime τ_n and give rise to a Class I spectrum.

The peak at λ = 4910 Å has been assigned to an exciton bound to a neutral donor. This is again consistent with our results since the peak appears after treatment at 180° C, when sufficient electrons from the desorbed oxygen have neutralized the donors in the surface near region, and is reduced by oxygen backfilling and IR irradiation. According to this, this donor could be a Cd interstitial or a S vacancy.

At higher treatment temperatures, the excess Cd distribution is homogenized due to Cd evaporation and some diffusion into the bulk, the accumulation layer is reduced, and the crystal becomes Class II. Competition between the above mentioned processes may explain the influence of the heating rate on the transition temperature. The anticoincidence between photocurrent and optical absorption would indicate the existence of a depletion layer in Class II CdS. It is not clear however how this depletion layer would arise as a consequence of heat treatments.

The increase in photocurrent and the decrease in green-edge emission that accompanies it, can be explained if one assumes with Spear and Bradberry (ref. 37) that the treatment introduces a slow recombination center, reducing the hole population in the centers that take part in the emission.

The long wavelength peak in the SDP at LNT (Figures 4.5.3-4 and 4.5.3-5) is not reduced by oxygen backfilling or IR irradiation and has no relation with the bound exciton peak at λ = 4910 Å. It arises because of a decrease in absorption towards lower energies.

In conclusion, the photoelectronic properties of a CdS crystal are dependent on the presence of a surface near layer, determined by the excess Cd distribution and the surface density of absorbed oxygen. Heat-treatments in UHV, causing oxygen desorption and homogenization of the excess Cd can change this surface near layer and thus the class (and photoconductive behavior) of the crystal.

4.6 Study of Intrinsic Defects in CdS Utilizing Radiation Damage

Combined with information from thermal damage and thermal desorption experiemtns, radiation damage studies have the potential of more clearly elucidating the intrinsic defect structure of CdS. The experimental techniques involved in the current studies are the measurement of the SDP and the TSC curves before and after X-irradiation. Supplementary information for the purpose of characterizing the crystals was obtained by determining the influence of oxygen, the lack of oxygen, and IR illumination on the photoelectronic properties.

In a previous report (ref. 6), the theoretical concepts involved, a review of the work that already has been done, and the experimental arrangement have been presented. Since that report, an additional paper on the annealing of electron-irradiated CdS has been published (ref. 38). In this work, charged centers produced by the irradiation (10 MeV electrons)

at LNT are annealed out in the temperature range 90° - 410° K. The two annealing stages take place between 130° - 230° K and 330° - 410° K. It is suggested that two kinds of radiation induced acceptors which also act as charged scattering centers begin to migrate in the two temperature ranges, a suggestion similar to that proposed by Böer, O'Connell and Schubert (ref. 39) and Böer and O'Connell (ref. 40).

Briefly, the procedure followed in the experiments is the following: 1) Characterization of the crystal (grown as described in Section 4.1) by SDP and TSC measurements, 2) irradiation with 150 keV (max) X-rays for one hour at room temperature, 3) immediate cooling to approximately LNT in order to freeze in any defects created, 4) within two hours, measurement of the SDP and TSC curves, and 5) annealing in the dark at room temperature for several days before retaking SDP and TSC measurements. In results presented in ref. 6, it had been found that X-irradiation did cause a change in both the SDP and TSC measurements obtained from a Class I crystal (see previous Section). In particular, the evidence seemed to indicate that the most dramatic change occurred after illuminating the crystal with extrinsic light ($\lambda > \lambda_{A\ \text{exciton}}$ or $\lambda_{B\ \text{exciton}}$ depending on whether polarization of the incident light was perpendicular or parallel to the c-axis of the CdS crystal). That is, after irradiation, the photocurrent obtained during measurement of the SDP was found to be only slightly increased over that obtained during the pre-irradiation measurement when the monochromator was scanned from shorter wavelengths ($\lambda \sim 4500$ Å) toward longer wavelengths ($\lambda \sim 5000$ Å). After extrinsic illumination, a scan over the same wavelengths would result in a substantial decrease in the SDP in the intrinsic range ($\lambda < \lambda_{A\ \text{exciton}}$ or $\lambda_{B\ \text{exciton}}$)-- this decrease being from 1/2 to one order of magnitude. Connected with this behavior seemed to be a shoulder in the SDP in the extrinsic region that was observable in the crystal both before and after irradiation. This shoulder decreased substantially in magnitude in the first scan of the SDP after-irradiation. In the second scan, it remained at approximately the same level as in the first scan (see Figure 4.6.1).

Because of this behavior, it was decided that further information was needed on the crystal, especially in the slightly extrinsic wavelength region. Using the same crystal as reported in ref. 6, but now in a higher conductivity state (ref. 6), measurements of the SDP were made at LNT and at a pressure of $\sim 10^{-3}$ torr. The results are seen in Figure 4.6.2. Curve 4.6.2-1 shows the existence of a photoconductivity peak due to the dissociation of bound excitons (maximum at ~ 4870 Å). It is known that some of the bound exciton states can be destroyed by IR light (refs. 41 and 42). Consequently, a SDP measurement at LNT was made with additional IR illumination (using a Unitron light source with an IR filter). These results are shown in curve 4.6.2-2. It is quite noticeable that the IR illumination partially quenched the intrinsic photoconductivity but totally destroyed the photoconductivity due to the bound exciton. Next, an IR monochromator was used to determine the wavelength response of the quenching of both the B exciton and the bound exciton. These results are seen in Figure 4.6.3.

Further experiments have indicated that it is necessary to illuminate the crystal at the bound exciton wavelength if the bound exciton photoconductivity peak is to be restored after IR illumination. This fact indicates that the bound exciton is not primarily located in the surface region accessible to intrinsic illumination. Additional studies are underway to further clarify this point.

At present, many questions remain as to the nature of the crystal being tested. The effect of IR illumination may be to ionize the center to which the exciton was previously bound, the idea being that with the changed charge state of the center the exciton will no longer be bound. However, it is presently unclear as to why such a wide range of wavelengths in the far visible and near infrared are capable of destroying the bound exciton photoconductivity. These and other questions must be answered in order to account for the changes induced by X-irradiation. In addition to further experiments at pressures of 10^{-3} torr, the crystal behavior will be examined at low pressures ($< 10^{-7}$ torr). With this information in hand, further irradiations will be made.

4.7 Investigation of the Effect of Growth Conditions on the Class of CdS Platelets

An investigation into the influence of growth conditions on the class (Class I or II as defined in Section 4.5) of the resulting crystals has been made. Crystals were grown in our laboratory using the technique described in Section 4.1. About 25 growing runs were made at relative concentrations of $[H_2S]:[N_2]$ ranging from 0 to 2.6%. After growth was complete the H_2S was left on until the crystals had cooled to a predetermined temperature. At this point, designated the turn off temperature, the H_2S was shut off. The crystals were then allowed to finish cooling with only the nitrogen carrier gas flowing. Turn off temperatures from room temperature to 500° C were used. Good platelets were obtained from all runs.

Depending on the H_2S concentration and turn off temperature, either Class I or Class II crystals resulted: For H_2S concentrations below 0.2% the crystals produced were always Class II, irrespective of the temperature at which the H_2S was turned off. This behavior for low H_2S concentrations is expected, since growth without H_2S produces Class II crystals. For H_2S concentrations above 0.2% and turn off temperatures above a critical temperature, Class I crystals resulted. For H_2S concentrations in this range Class II crystals were produced if the H_2S turn off temperature was below the critical temperature. This transition temperature below which Class II crystals were produced and above which Class I crystals were produced increases with increased H_2S concentration. At 0.25% H_2S concentration the transition temperature was 200° C. At 2.6% H_2S concentration it is above 350° C. The above data are summarized in Figure 4.7.1.

The highest turn off temperature used in the above work was 500° C. A set of five runs has also been made with a turn off temperature of 1050° C.

This turn off temperature resulted from turning the H_2S off immediately after completion of the growth run, just as the crystals began to cool. Crystals grown at H_2S concentrations of 0.3% H_2S and lower were Class II. Those grown at 0.6% were Class I. At these high temperatures it would appear, therefore, that the transition line between classes has shifted to higher H_2S concentrations. This is probably due to a partial re-establishment of equilibrium between the crystal bulk and the surrounding lower H_2S concentration before the temperature falls enough to prevent diffusion. The crystals therefore take on the characteristics of a lower H_2S concentration.

The dividing line between Class I and Class II in Figure 4.7.1 is also a function of crystal thickness. Within a given run, if it is carried out under conditions near the transition line, crystals of both classes may be found. The thicker ones will be Class II, the thinner, Class I. This is as we would expect since surface effects become more significant as crystal thickness decreases.

Most important, however, was the atmosphere sensitivity exhibited by some of these crystals. Sensitivity to ambient on the part of Class I crystals is well known (refs. 6 and 31). Class II crystals are normally insensitive to ambient. However, crystals grown at high H_2S concentrations and cooled to low turn off temperatures were found to be atmosphere sensitive. Under a vacuum of 10^{-3} torr these crystals, which were Class II at 1 atmosphere of air, became Class I. Upon re-exposure to air they reverted to Class II. Classification based on the exciton absorption spectra was used for one crystal in this group and confirmed the assignment to Class I made on the basis of the room temperature SDP (see Section 4.5). It is clear from these initial results that both Class I and Class II crystals grown in high H_2S concentrations are sensitive to ambient. These crystals must be avoided in applications where insensitivity to atmosphere is important. It is also clear that just specifying that the crystals must be Class II is insufficient; atmosphere sensitivity can only be avoided by careful control of the H_2S level or further treatment of the crystals after growth.

5. CONCLUSIONS

The work performed under this contract, aimed at increasing our knowledge about the Cu_xS:CdS photovoltaic cell and thus leading to the enhancement of cell performance, has produced the following results and conclusions:

a. Quenching studies on doped CdS crystals have led to further understanding of the acceptor levels which affect the photoelectronic behavior of Cu_xS:CdS photovoltaic cells.

b. Theoretical investigations have led to the development of a comprehensive model for the Cu_xS:CdS photovoltaic cell. Although the model is undergoing further development, its main features can be outlined:

   1. The electron affinity of CdS is 0.35 eV larger than that of Cu_2S.

   2. Electron traps between 0.2 eV and 0.65 eV below the CdS conduction band affect tunneling current under low forward bias and some aspects of the dependence of V_{oc} on illumination intensity.

   3. Acceptor levels resulting from Cu diffused into the CdS during heat treatment create a compensated CdS layer. Detailed consideration of the effects of these levels leads to explanations of observed enhancement and quenching and the effect of heat treatment.

   4. Recombination centers at the Cu_xS:CdS interface affect tunneling currents at low forward bias, the cell fill factor, and the maximum V_{oc} and its dependence on illumination.

   The unified model reconciles the disagreements between the Stanford and Clevite models and accounts for previously unexplained experimental results. The success of the unified model is felt to be related to its detailed consideration of the level structure in the band gap, thus emphasizing the importance of studies of these levels and the defects they are due to.

d. Experimental studies indicate that the dip in the spectral response of Cu_xS:CdS photovoltaic cells near the band edge of CdS is due to a trap-controlled mechanism in the CdS.

e. Further consideration of the interlayer model (ref. 6) has led to the suggestion that the high open-circuit voltage observed by Chamberlin and Skarman (ref. 18) on some Cu_xS:CdS cells is due to the fact that the Cu_xS layer consists of djurleite.

f. Consideration of the effects of a short heat treatment in air at ~ 200 - 250° C of Cu_xS:CdS cells has led to the conclusion that a recrystallization of the initial CdS layer, possibly by adapting the method described by Böer et al (ref. 28), would enhance cell performance.

g. In order that cells be stable with respect to oxygen ambient the surface-near region of the CdS should be less Cd-rich than the bulk. This substantiates preliminary results.

h. Radiation-damage studies have given preliminary information on exciton behavior.

i. The conditions under which CdS crystals with different photoelectronic properties are grown have been empirically determined with respect to ambient atmosphere and temperature during cool-down.

j. Insensitivity of CdS crystals to oxygen ambient is enhanced by using low H_2S concentrations during growth.

6. REFERENCES

1. R. H. Bube, Photoconductivity of Solids, J. Wiley & Sons, New York, N.Y. (1960).

2. G. A. Dussel and K. W. Böer, Field Quenching as a Mechanism of Negative Differential Conductivity in Photoconducting CdS, Phys. Stat. Sol. 39, 391 (1970).

3. G. A. Dussel and K. W. Böer, Field Enhanced Ionization, Phys. Stat. Sol. 39, 375 (1970).

4. K. W. Böer, Layerlike Field Inhomogeneities in Homogeneous Semiconductors in the Range of N-Shaped Negative Differential Conductivity, Phys. Rev. 139,6A, 1949 (1965).

5. K. W. Böer, G. Döhler, G. A. Dussel and P. Voss, Experimental Determination of Changes in Conductivity with Electric Field Using a Stationary High Field Domain Analysis, Phys. Rev. 169, 700 (1968).

6. K. W. Böer, Research Study of the Photovoltaic Effect in CdS, Final Report, NASA-JPL Contract No. 952666, October 1970.

7. C. B. Burgett and C. C. Lin, Infrared Quenching of the Luminescence and Photohall Effect of ZnS:Cu and CdS:Cu Crystals, J. Phys. Chem. Sol. 31, 1353 (1970).

8. M. I. Kolinin, Structure of Photosensitivity Centers in CdS Crystals, Soviet Phys. 4, 1368 (1971).

9. L. R. Shiozawa, G. A. Sullivan, F. Augustine, J. M. Smith III, and W. R. Cook, Jr., Research on the Mechanism of the Photovoltaic Effect in High-Efficiency CdS Thin-Film Solar Cells, Final Report, Contract AF33(615)-5224 (1969).

10. W. D. Gill, Photovoltaic Properties of Cu_2S:CdS Heterojunctions, Ph.D. Thesis, Stanford University (1969).

11. W. D. Gill and R. H. Bube, Photovoltaic Properties of Cu_2S-CdS Heterojunctions, J. Appl. Phys. 41, 3731 (1970).

12. R. H. Bube, Mechanism of the Photovoltaic Effect in II-VI Compounds, Progress Report No. 9, Grant NGR-05-020-214 S-1, April 1-June 30, 1970, also
P. F. Lindquist, Mechanism of the Photovoltaic Effect in II-VI Compounds, Ph.D. Thesis, Stanford University (1970). (Available as Progress Report No. 9, Grant NGL-05-020-214 S-1, NASA-Lewis, R. H. Bube, Principal Investigator, June (1970)).

13. A. E. Potter, Jr. and R. L. Schalla, Mechanism of Cadmium Sulfide Film Cell, Conference Record of the Sixth Photovoltaic Specialists Conference, Vol. 1, p. 24 (1967).

14. H. W. Brandhorst, Jr., R. L. Schalla, A. E. Potter, Jr., and L. Rosenblum, Effects of Bias Light and Heat Treatment on the Spectral Response of Cadmium Sulfide Thin Film Photovoltaic Cells, NASA Technical Note, NASA TN D-5521.

15. S. Martinuzzi, et al., Hall Effect Measurements on Cu_2S Layers, Phys. Stat. Sol. (a) 2, K9 (1970).

16. P. N. Keating, Photovoltaic Effects in Photoconductors, J. Appl. Phys. 36, No. 2, 564 (1965).

17. Ref. 1, p. 242.

18. R. R. Chamberlin and J. S. Skarman, Chemically-Sprayed Thin-Film Photovoltaic Converters, Sol. St. Electronics 9, 819 (1966).

19. J. S. Skarman, A. B. Budinger, R. R. Chamberlin, Investigation of Chemically-Sprayed Thin-Film Photovoltaic Cells, Summary Report, Contract AF 33(615)-1578, Aero Propulsion Lab., June 1965.

20. Ibid, p. 18

21. N. Nakayama, Ceramic CdS Solar Cell, Jap. J. Appl. Phys. 8, 450 (1969).

22. N. Miya, Cu_xS-CdS Junction Cell for the C-Plane of the CdS Single Crystal, Jap. J. Appl. Phys. 9, 768 (1970).

23. M. C. Sneed, J. L. Maynard, and R. C. Brasted, Eds., Comprehensive Inorganic Chemistry, Vol. 2, van Nostrand, New York (1954).

24. R. H. Bube, P. F. Lindquist, and K. Muray, Mechanism of the Photovoltaic Effect in II-VI Compounds, Progress Report No. 6, Grant NGR-05-020-214 S-1, NASA-Lewis, Sept. 1969.

25. Reference 9, p. 83.

26. J. M. Gilles and J. Van Cakenberghe, Photoconductivity and Crystal Size in Evaporated Layers of Cadmium Sulphide, Nature 182, 862 (1958).

27. P. A. Crossley, C T. Noel, M. Wolf, Review and Evaluation of Past Solar Cell Development Efforts, Final Report on Contract No. NASW-1427, RCA for NASA, June 1968.

28. K. W. Böer, A. S. Esbitt, and W. M. Kaufman, Evaporated and Recrystallized CdS Layers, J. Appl. Phys. 37, 2664 (1966); K. W. Böer, J. W. Feitknecht, and D. G. Kannenberg, Properties of Recrystallized Evaporated CdS Layers, Phys. Stat. Sol. 16, 697 (1966).

29. J. J. Loferski, Theoretical Considerations Governing the Choice of the Optimum Semiconductor for Photovoltaic Solar Energy Conversion, J. Appl. Phys. 27, 777 (1956).

30. E. F. Gross et al., The Investigation by the Photoconductivity and Luminescence Method of the Exciton States new the Edge in the Depth of the Fundamental Absorption in Crystals, Proc. of the 7th Int. Conf. on Semiconductors, p. 5, Paris (1964).

31. R. Schubert and K. W. Böer, Desorption of Oxygen and Its Influence on the Electrical Properties of CdS Single Crystal Platelets, J. Phys. Chem. Sol. 32, 77 (1971).

32. J. A. Bragagnolo and K. W. Böer, Luminescence Spectrum of Undoped CdS Platelets as a Function of Slight Heat-Treatment in Ultra-high Vacuum, J. of Luminescence 1, 572 (1970).

33. D. C. Reynolds, C. W. Litton and T. C. Collins, Some Optical Properties of Group II-VI Semiconductors (I), Phys. Stat. Sol. 9, 645 (1965).

34. P. Mark, Ambipolar Diffusion of Free Carriers in Insolating CdS Crystals, Phys. Rev. 137A, 203 (1965).

35. E. H. Weber, Zusammenhang Zwischen Baumladung, Oberflächenleitfähigkeit und Bandverbiegung für Photoleiter bei homogener Optischer Anregung, Phys. Stat. Sol. 17, 843 (1966).

36. J. Voigt and E. Ost, On the Dynamical Behavior of Exciton in CdS Single Crystals, Phys. Stat. Sol. 33, 381 (1969).

37. W. E. Spear and G. W. Bradberry, The Edge Emission in CdS Crystals, Phys. Stat. Sol. 8, 649 (1965).

38. M. Kitagawa and T. Yoshida, Annealing of Electron Irradiated CdS, Appl. Phys. Lett. 18, 41 (1971).

39. K. W. Böer, J. C. O'Connell, and R. Schubert, X-Ray Damage and Annealing of These Defects in CdS Single Crystals, Proc. of the Int. Symp. on Luminescence, Munich, 1965 (Verlag Karl Thiemig KG, Münich, 1966), p. 223.

40. K. W. Böer and J. C. O'Connell, Intrinsic Point Defects in CdS, Proc. of the Int. Conf. on Luminescence, Budapest, 1966 (Hungarian Academy of Sciences, Budapest, 1968), p. 1063.

41. D. G. Thomas and J.J. Hopfield, Optical Properties of Bound Exciton Complexes in Cadmium Sulfide, Phys. Rev. 128, 2135 (1962).

42. Y. Fujishiro and H. Mitsuhashi, Luminescence and Photoconductivity of CdS Single Crystals, Proc. of the Int. Conf. on Luminescence, Budapest, 1966 (Hungarian Academy of Sciences, Budapest, 1968), p. 1056.

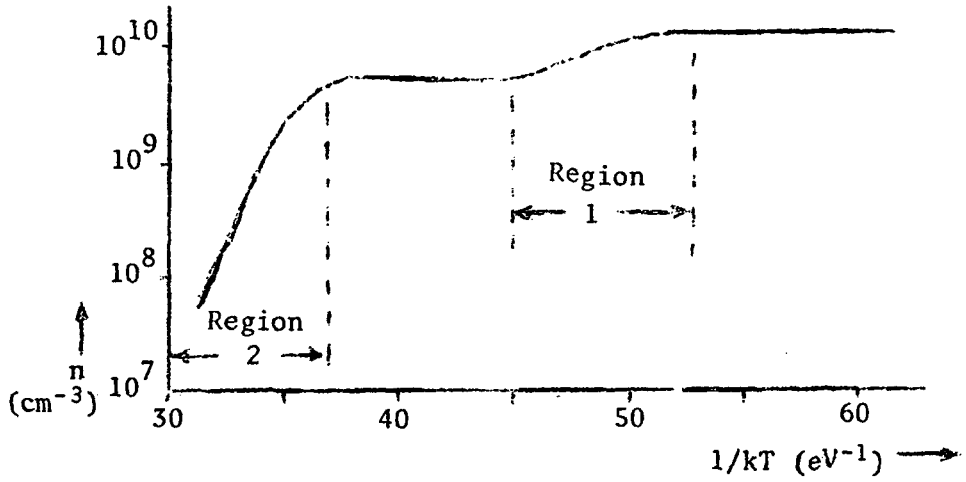

FIGURE 4.1.1: Thermal Quenching

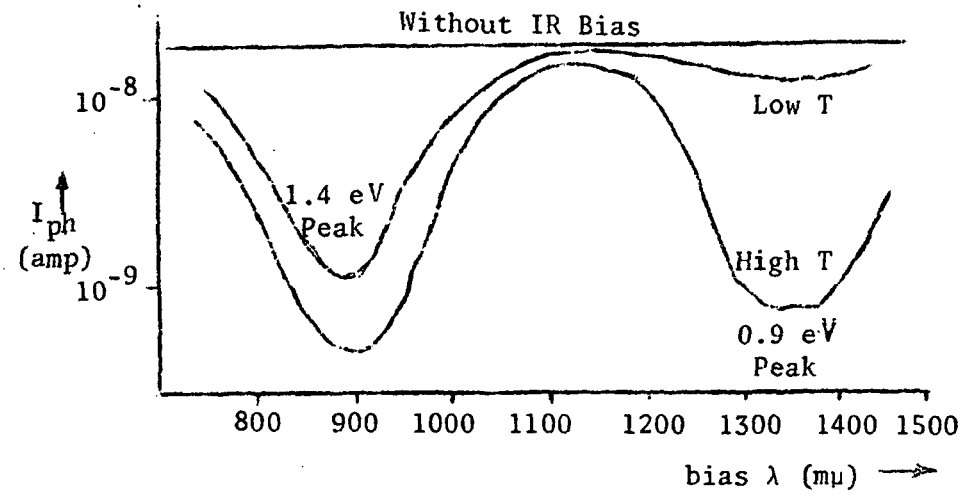

FIGURE 4.1.2: Infrared Quenching

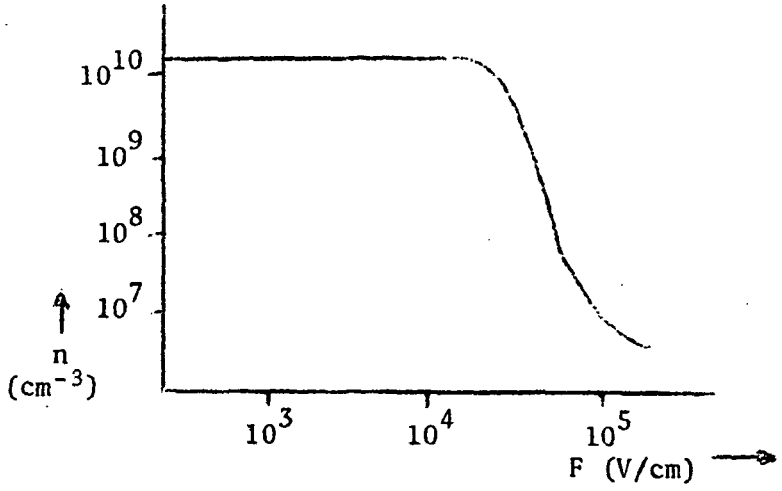

FIGURE 4.1.3: Field Quenching

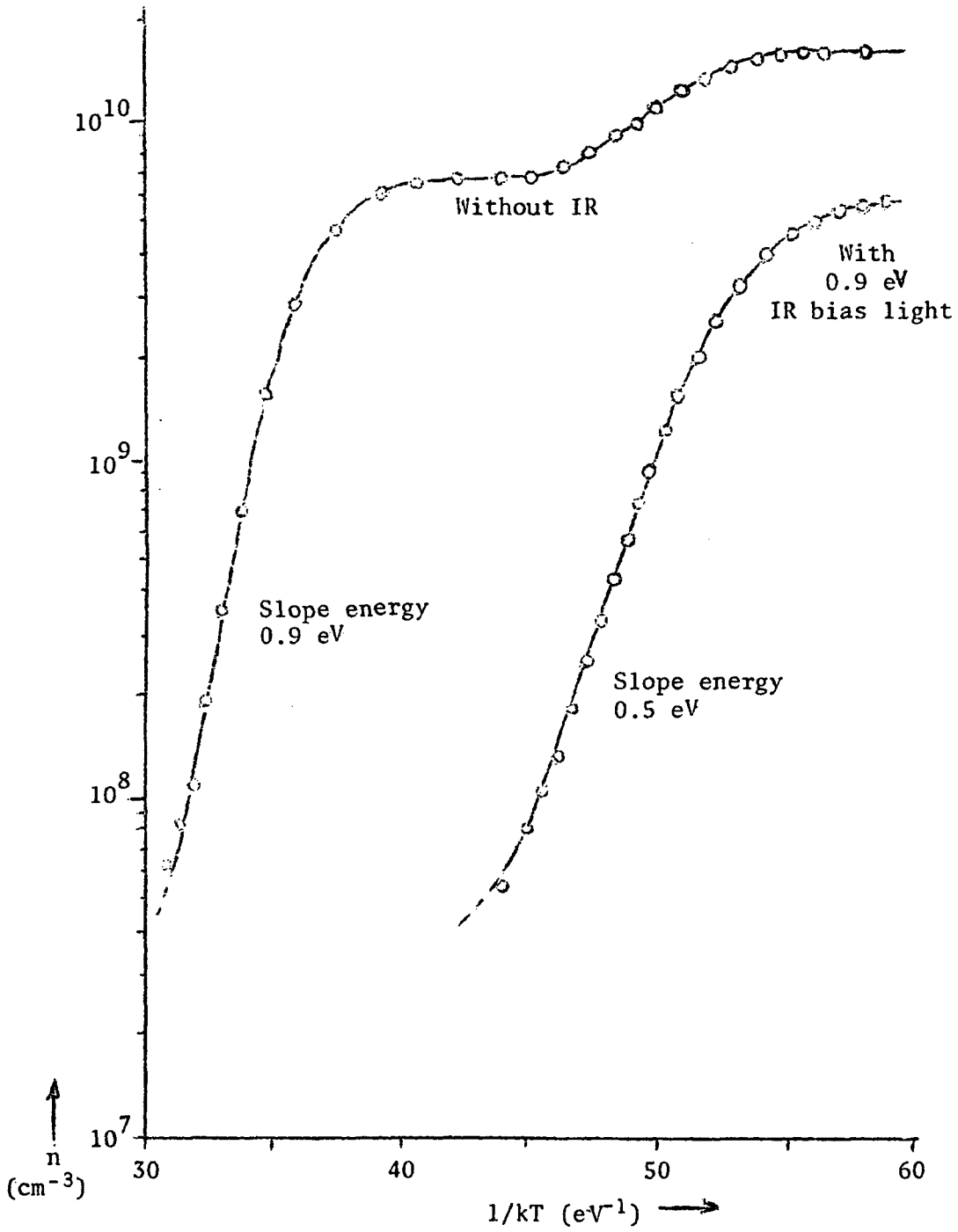

FIGURE 4.1.4: Thermal Quenching With 0.9 eV Bias Light

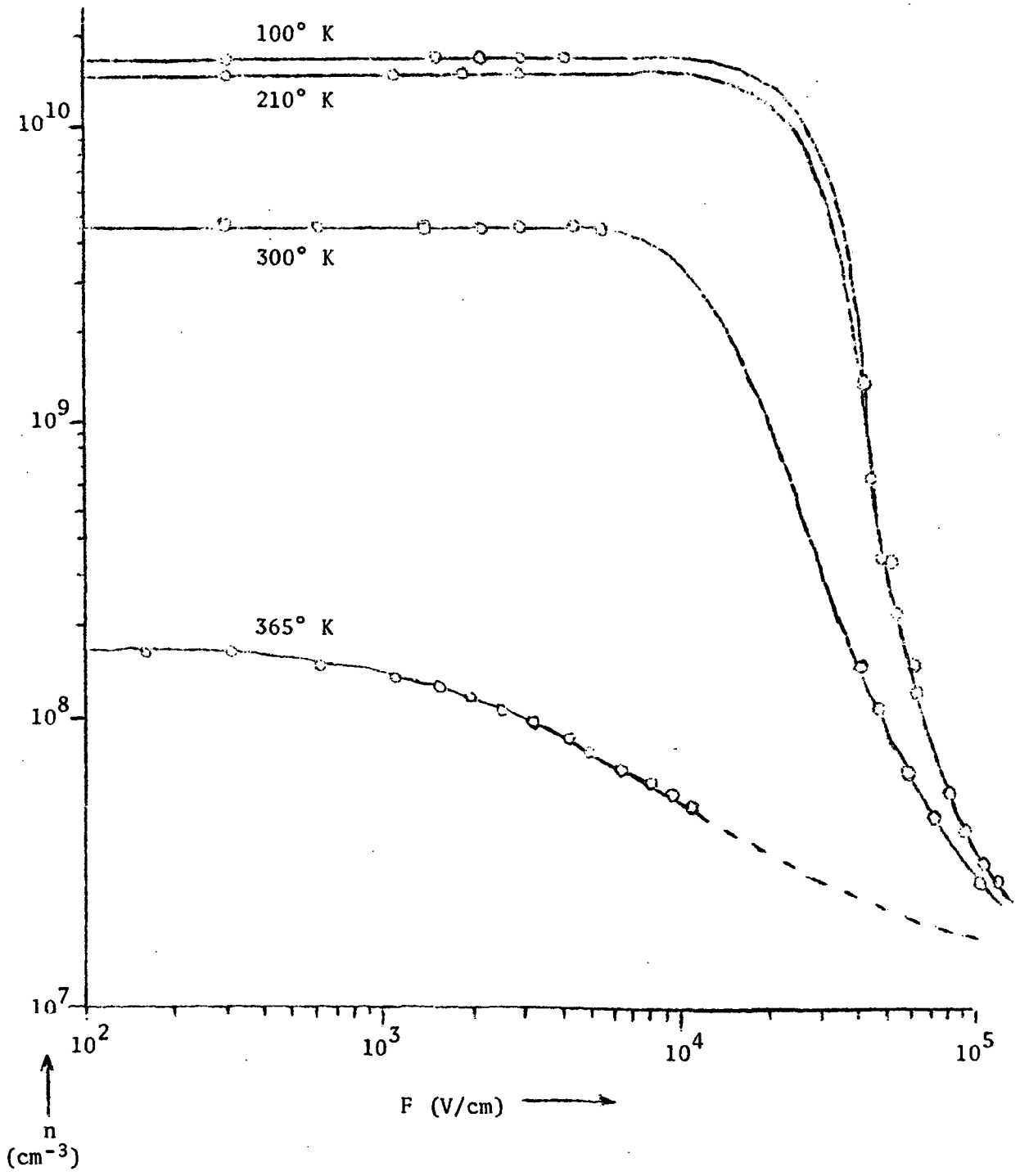

FIGURE 4.1.5a: Thermal Quenching Effect on Field Quenching

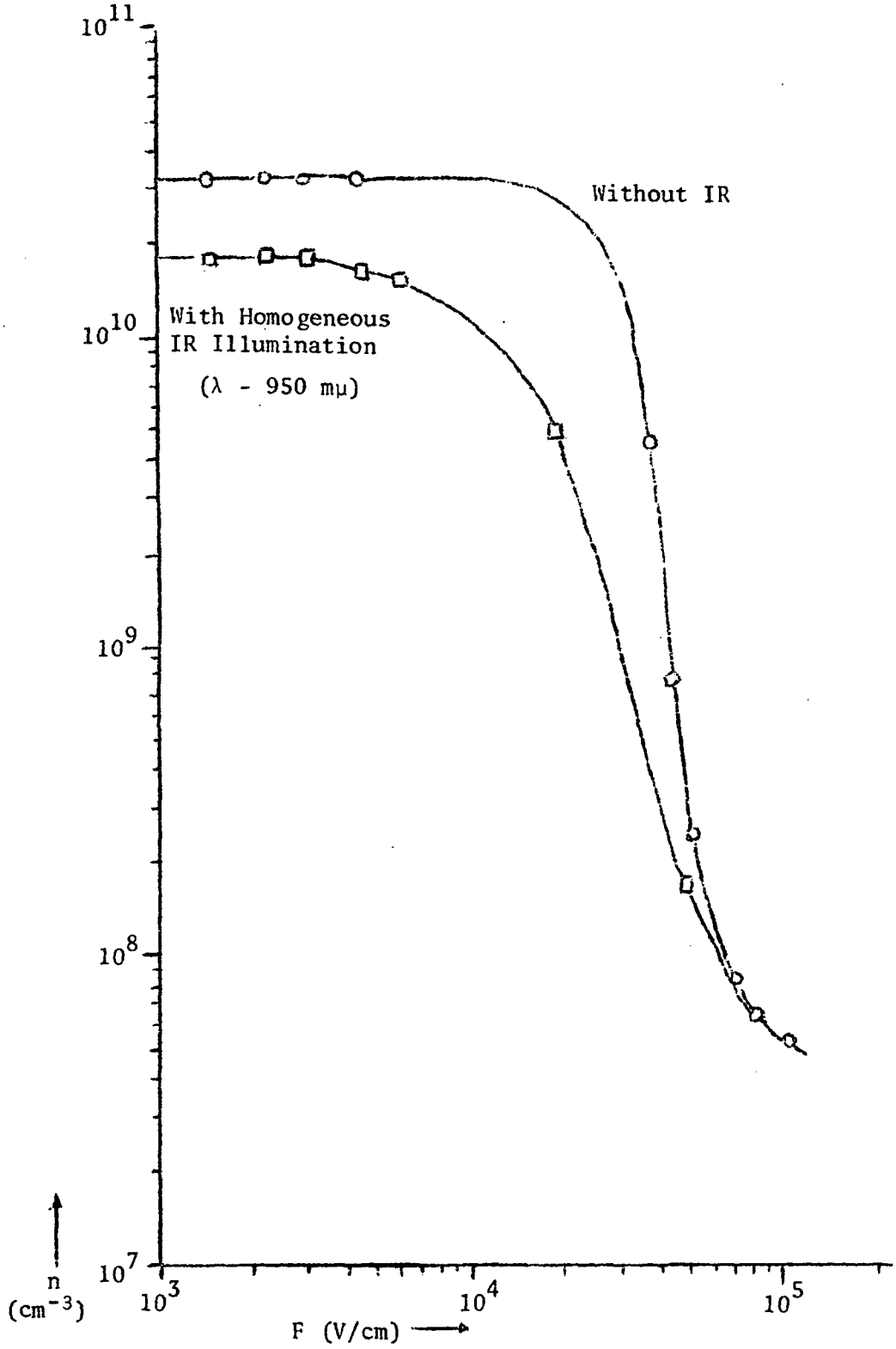

FIGURE 4.1.5b: IR Quenching Effect on Field Quenching

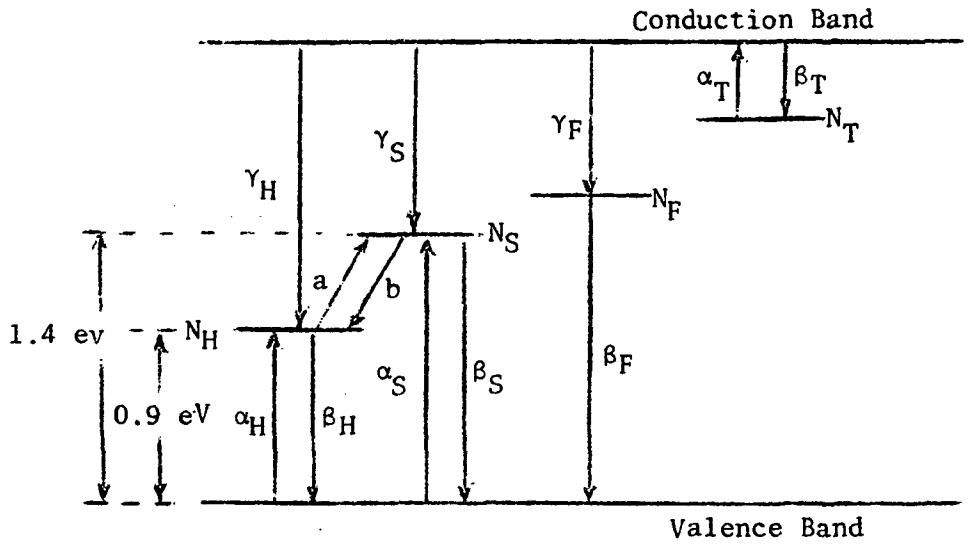

N_T = Electron Trap Density

N_F = Fast Recombination Center Density

N_S, N_H = Slow Recombination Centers Densities

α_T = Ionization Probability for Electrons to C.B.

α_S, α_H = Ionization Probabilities for Holes to V.B.

β_T = Capture Cross Section for Electrons from C.B.

β_S, β_H, β_F = Capture Cross Section for Holes from V.B.

a = Ionization of Holes from S to H Centers

b = Capture of Holes from H to S Centers

FIGURE 4.1.6: Level Structure for CdS:Ag,Al or CdS:Cu

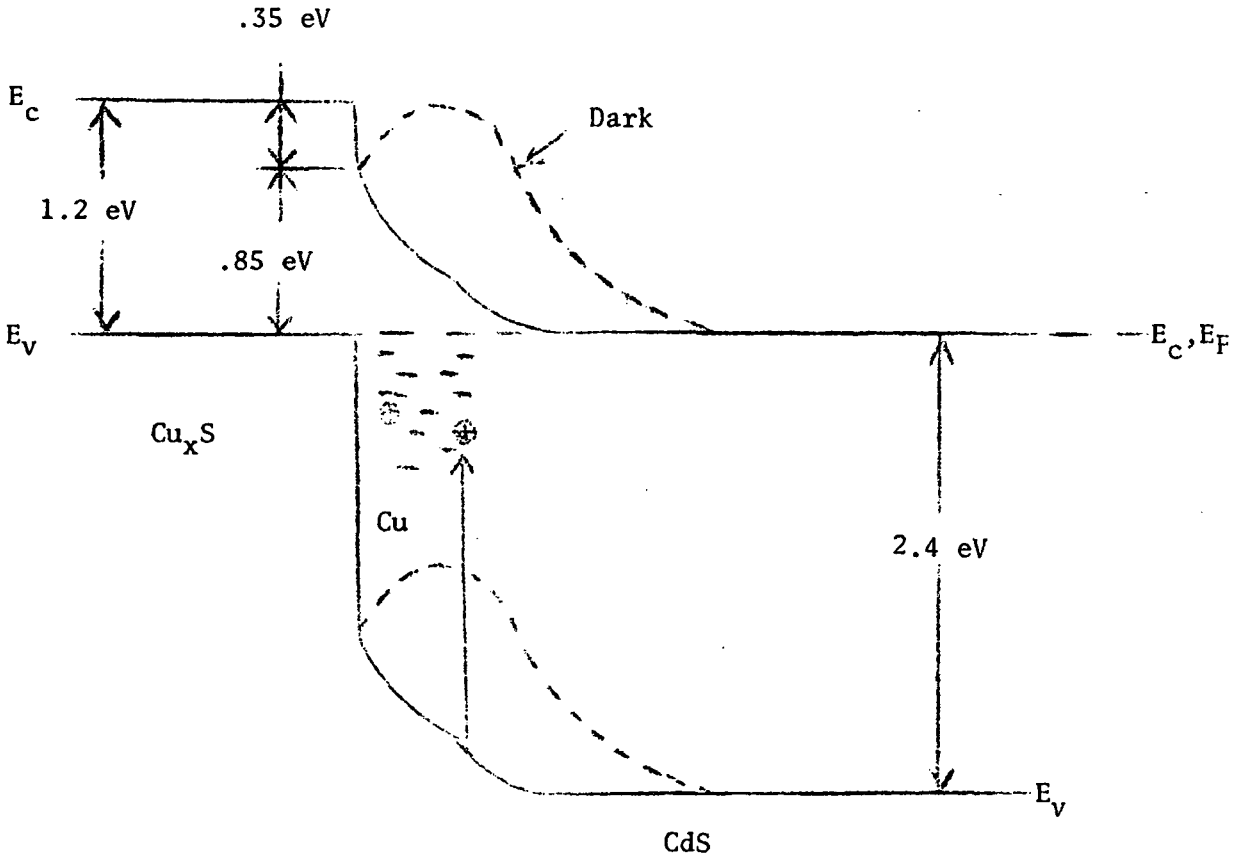

FIGURE 4.2.1: Band Diagram for the Clevite Model. After Ref. 9.

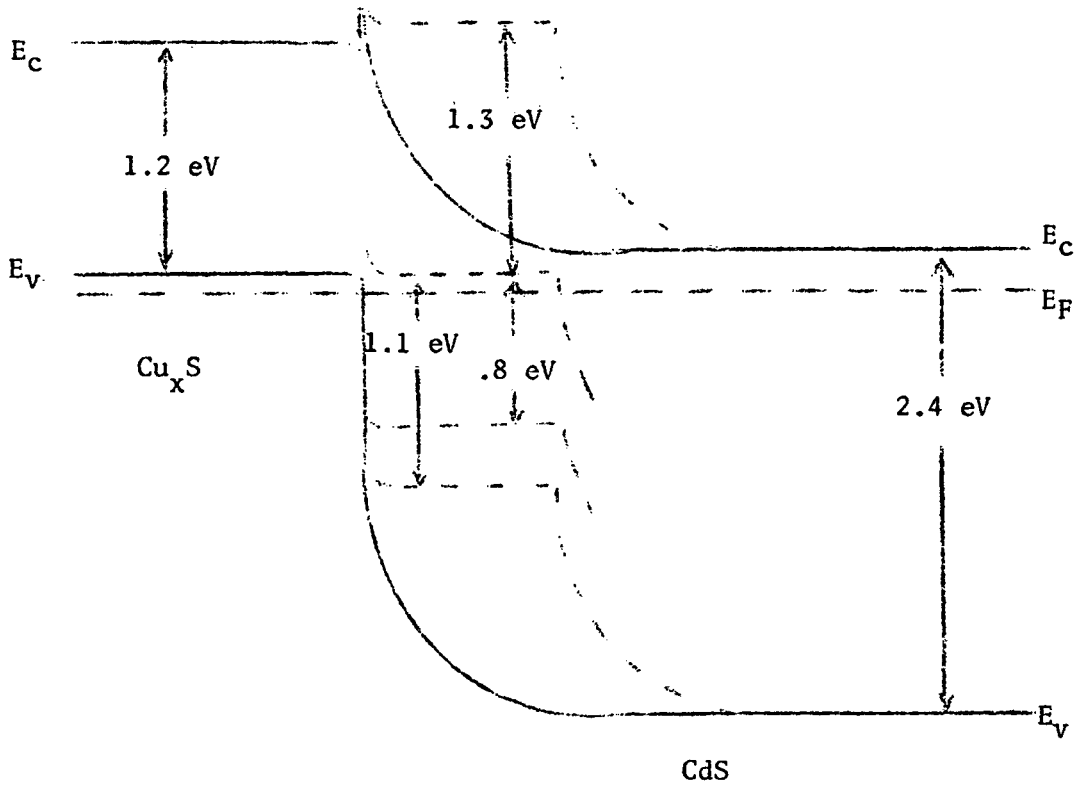

FIGURE 4.2.2: Band Diagram for the Stanford Model. After Ref. 10.

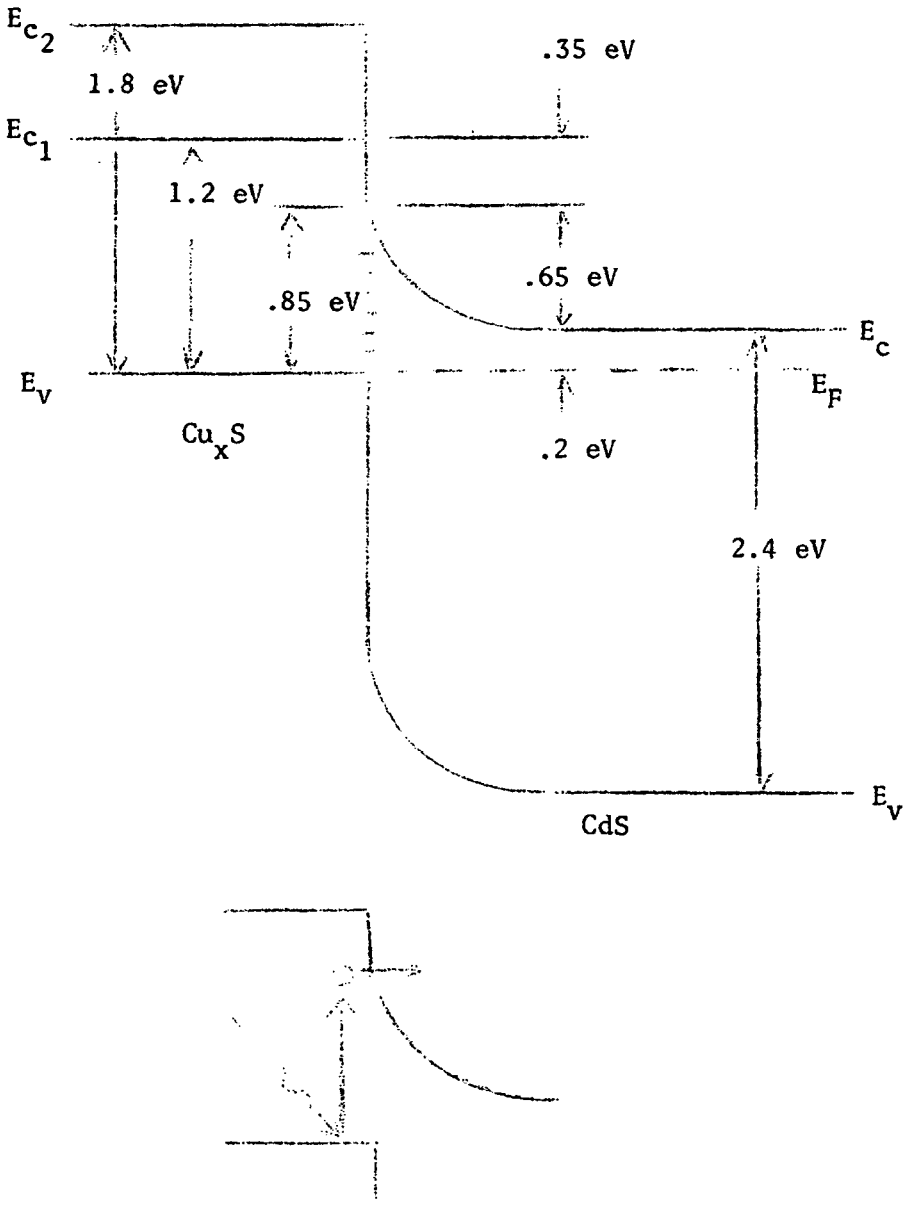

FIGURE 4.2.3: Band Diagram Similar to Clevite Model Without Heat Treatment.

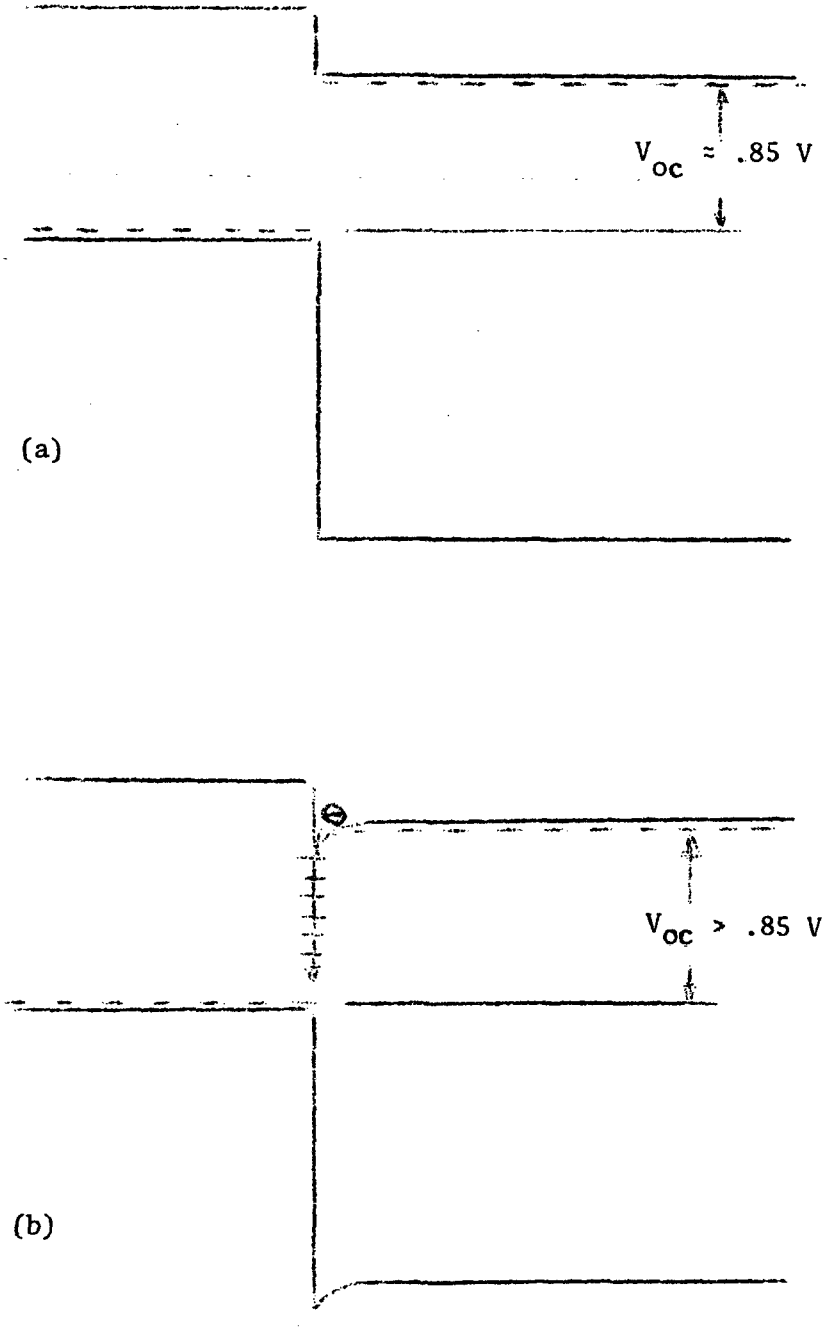

FIGURE 4.2.4: Illustration of Explanation for Maximum V_{oc}. (a) Maximum V_{oc} = 0.85 V, (b) Recombination at the Interface Opposes an Attempt to Increase V_{oc} above 0.85 V.

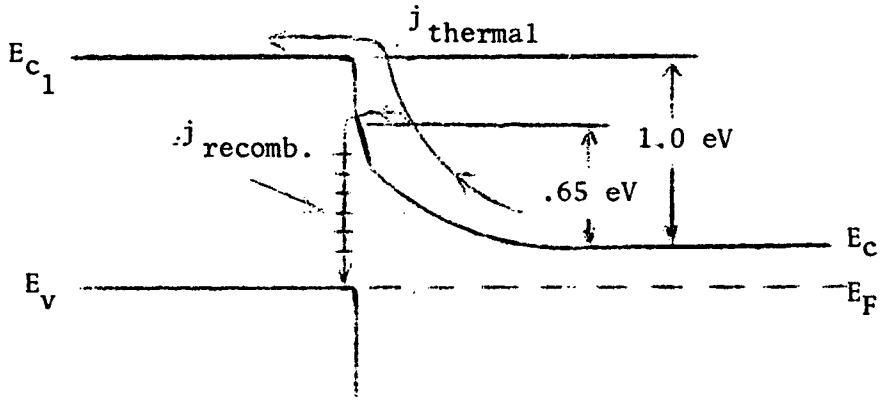

FIGURE 4.2.5: Diagram of Conduction Band Showing the Two Paths of Current Under Forward Bias.

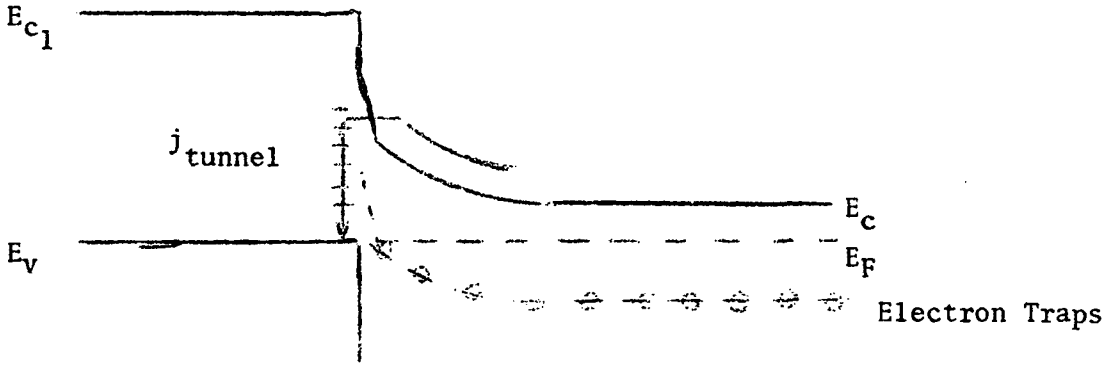

FIGURE 4.2.6: Tunneling Currents to Interface States.

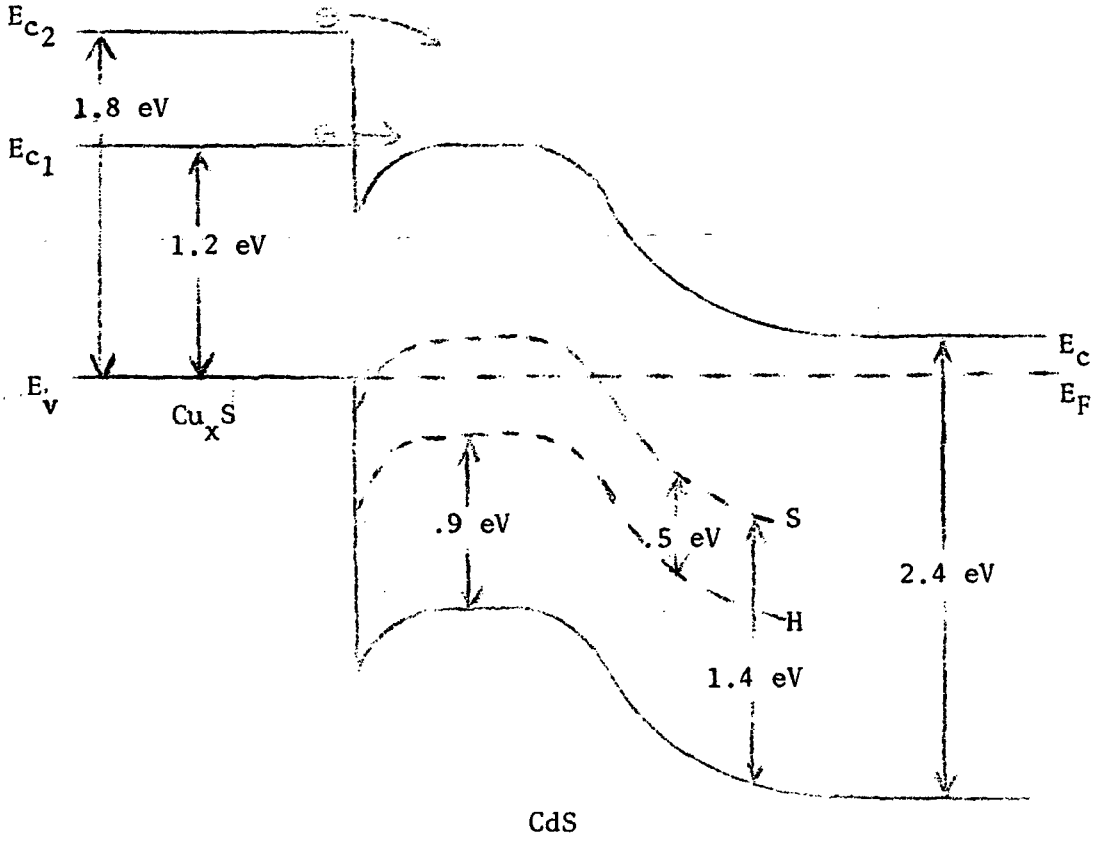

FIGURE 4.2.7: Band Diagram After Heat Treatment.

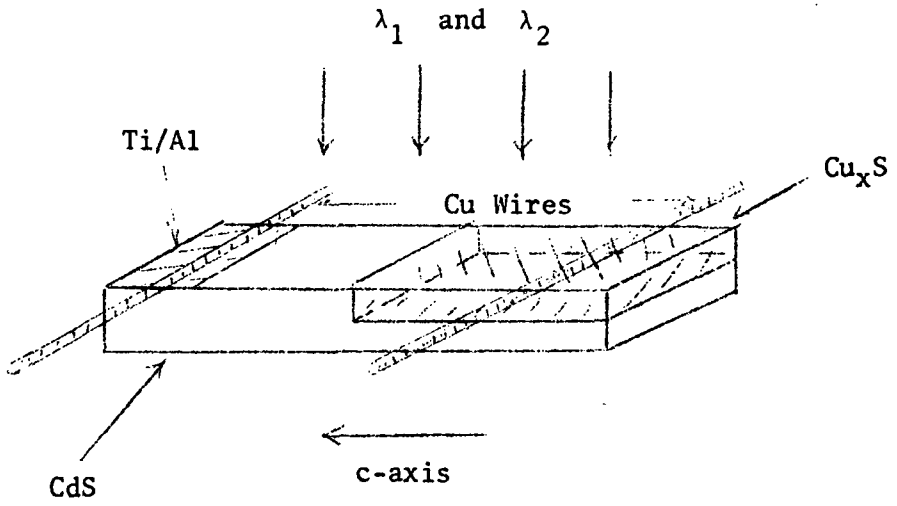

FIGURE 4.3.1: Schematic Cell Geometry

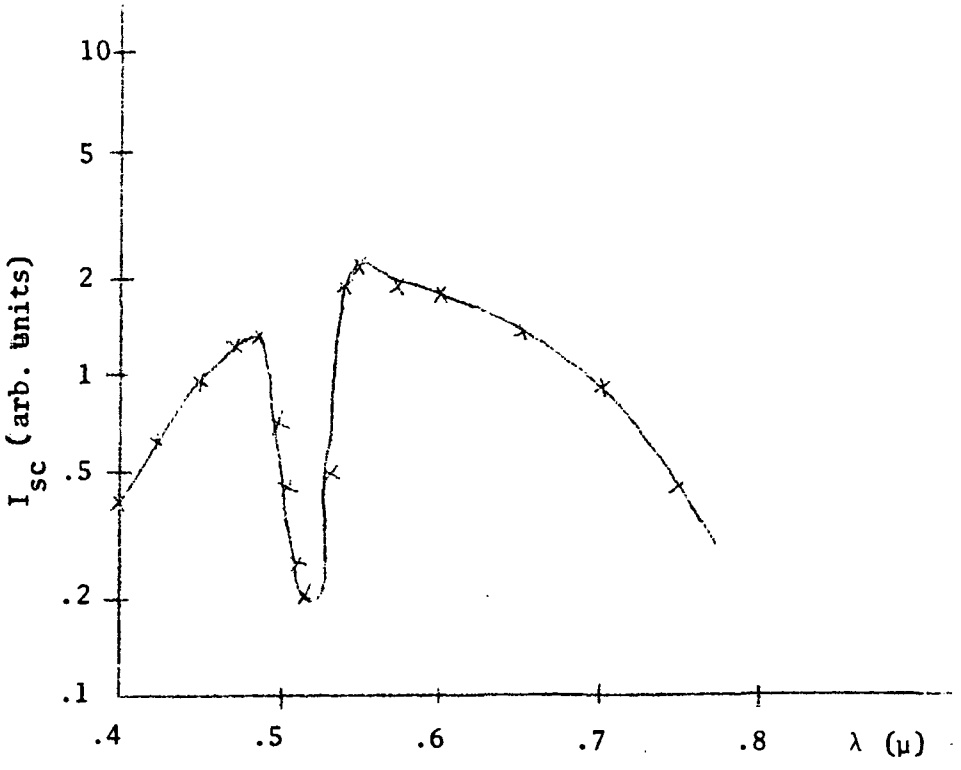

FIGURE 4.3.2: I_{sc} vs. λ for One Light Source

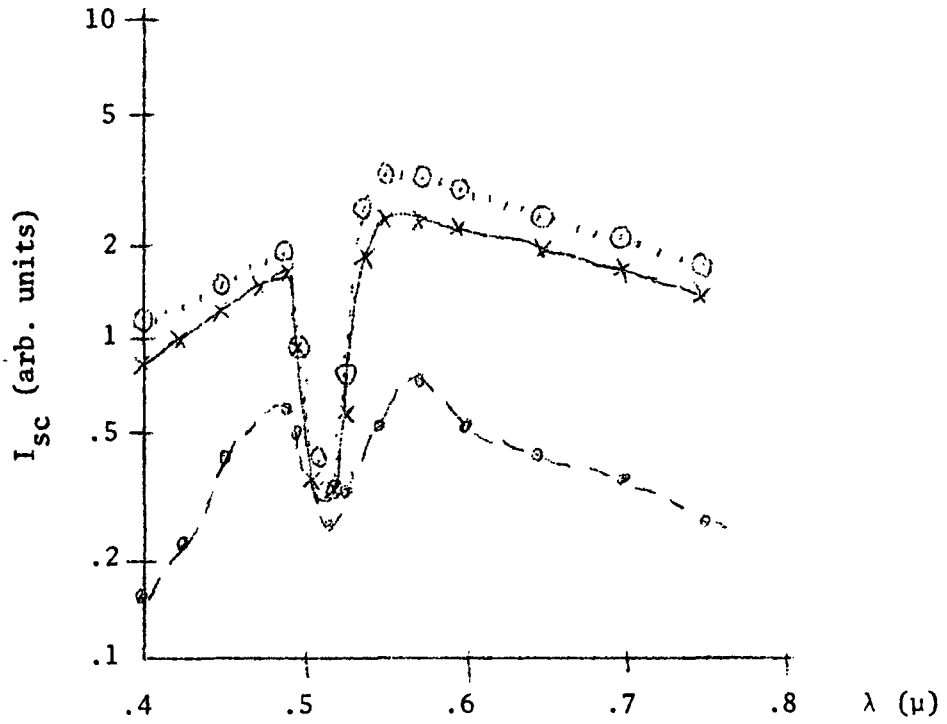

FIGURE 4.3.3: I_{sc} vs. λ_1 for Two Light Sources (Unnormalized)

λ_1 = 0.5 μ

λ_1 = 0.515 μ

λ_1 = 0.6 μ

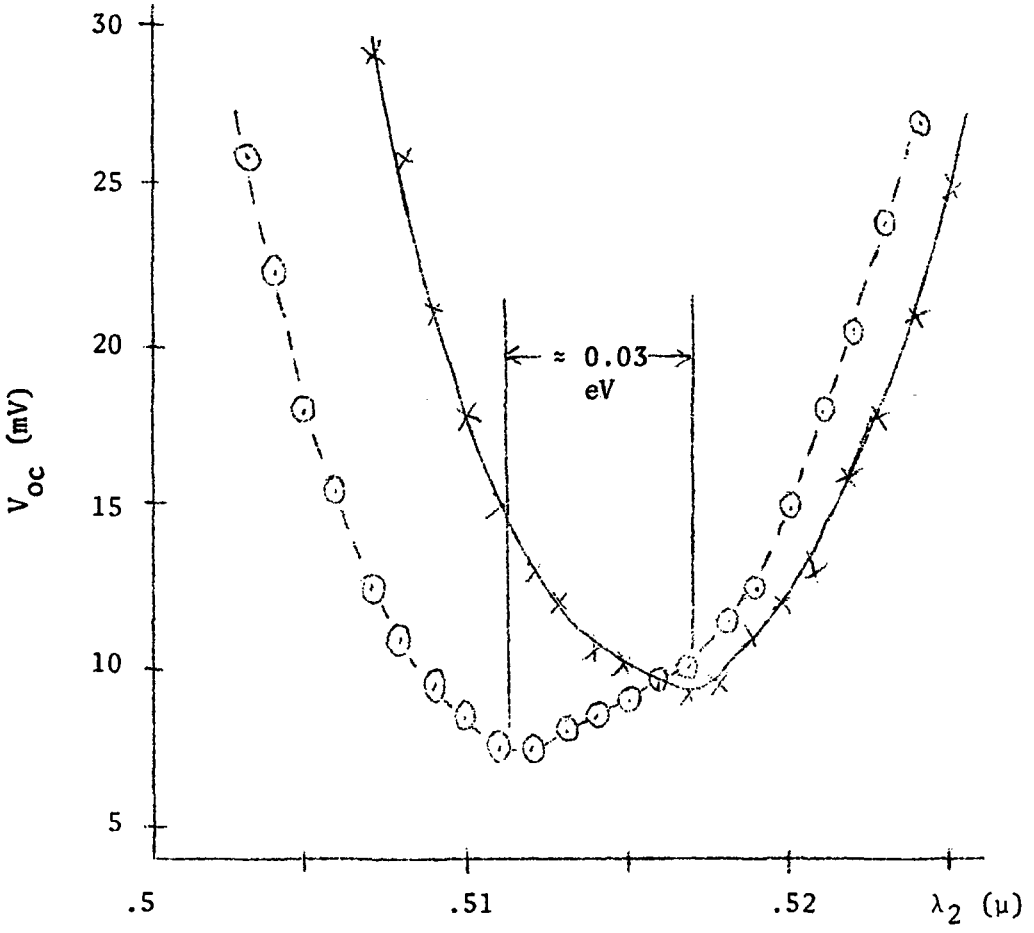

FIGURE 4.3.4: V_{oc} vs. λ_1 (polarized)
For λ_2 = 0.6 μ (unpolarized)

E ⊥ c

E ∥ c

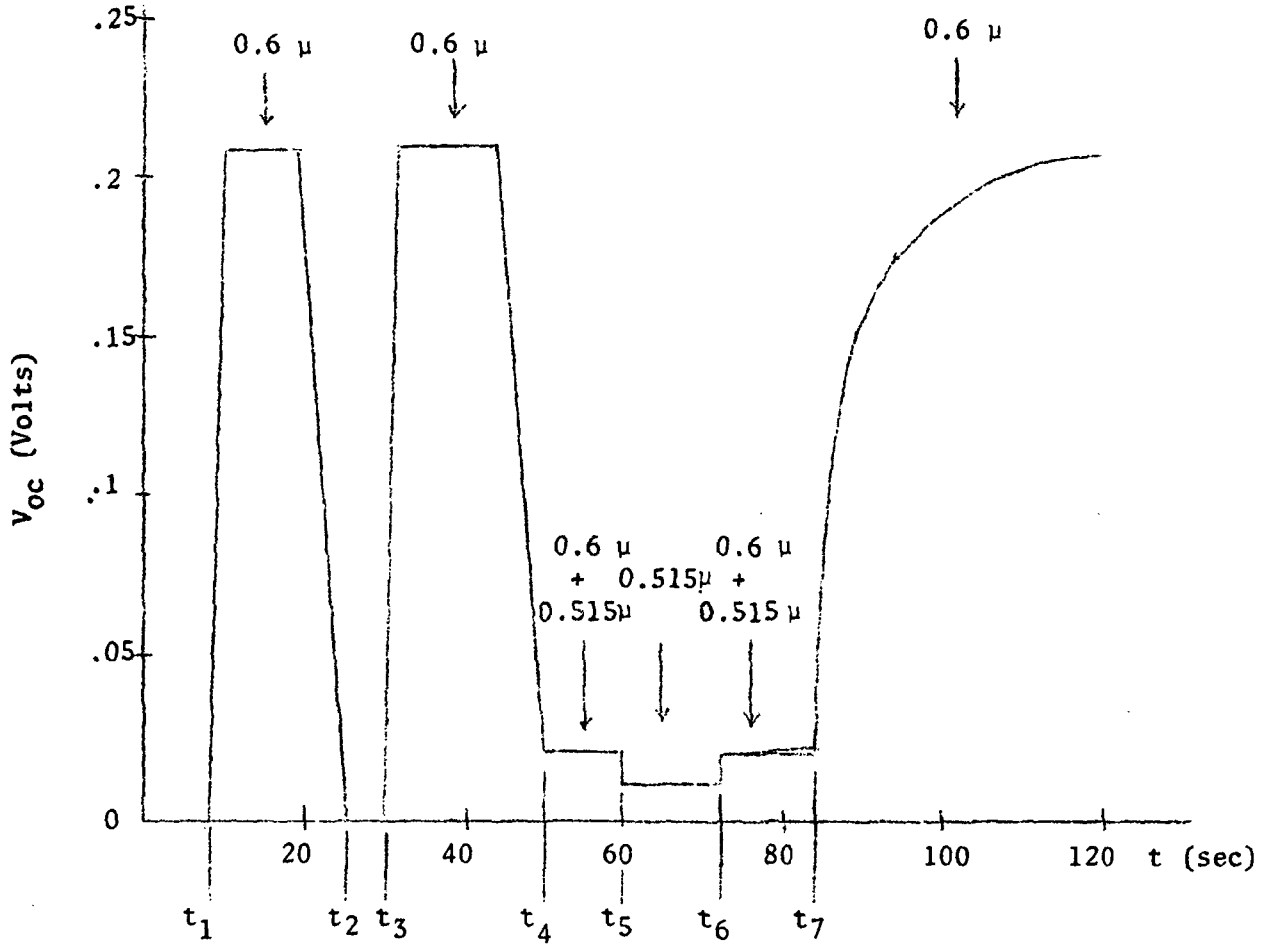

FIGURE 4.3.5: V_{oc} vs. Time for Two Sources with 0.515 μ Illuminating only CdS and Junction and 0.6 μ Source Over Entire Cell

t = 0 Both Sources Off

t_1: 0.6 μ Source On

t_2: 0.6 μ Source Off

t_3: 0.6 μ Source On

t_4: 0.6 μ Source On and 0.515 μ Source On

t_5: 0.6 μ Source Off and 0.515 μ Source On

t_6: 0.6 μ Source On and 0.515 μ Source On

t_7: 0.6 μ Source On and 0.515 μ Source Off

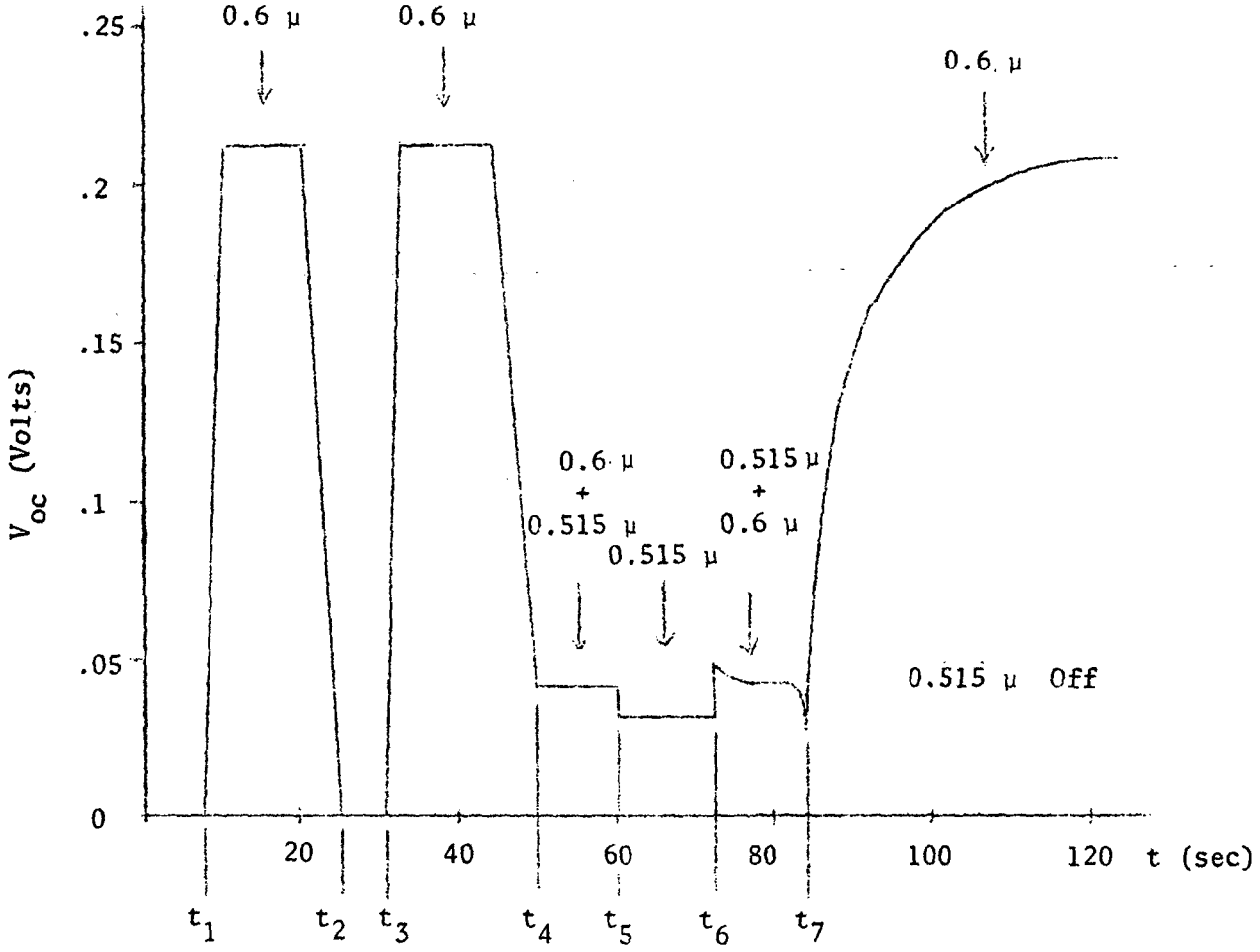

FIGURE 4.3.6: V_{oc} vs. Time for Two Source With 0.515 μ and 0.6 μ Illuminating Entire Cell. See Figure 4.3.5 for Explanation of t_1 through t_7.

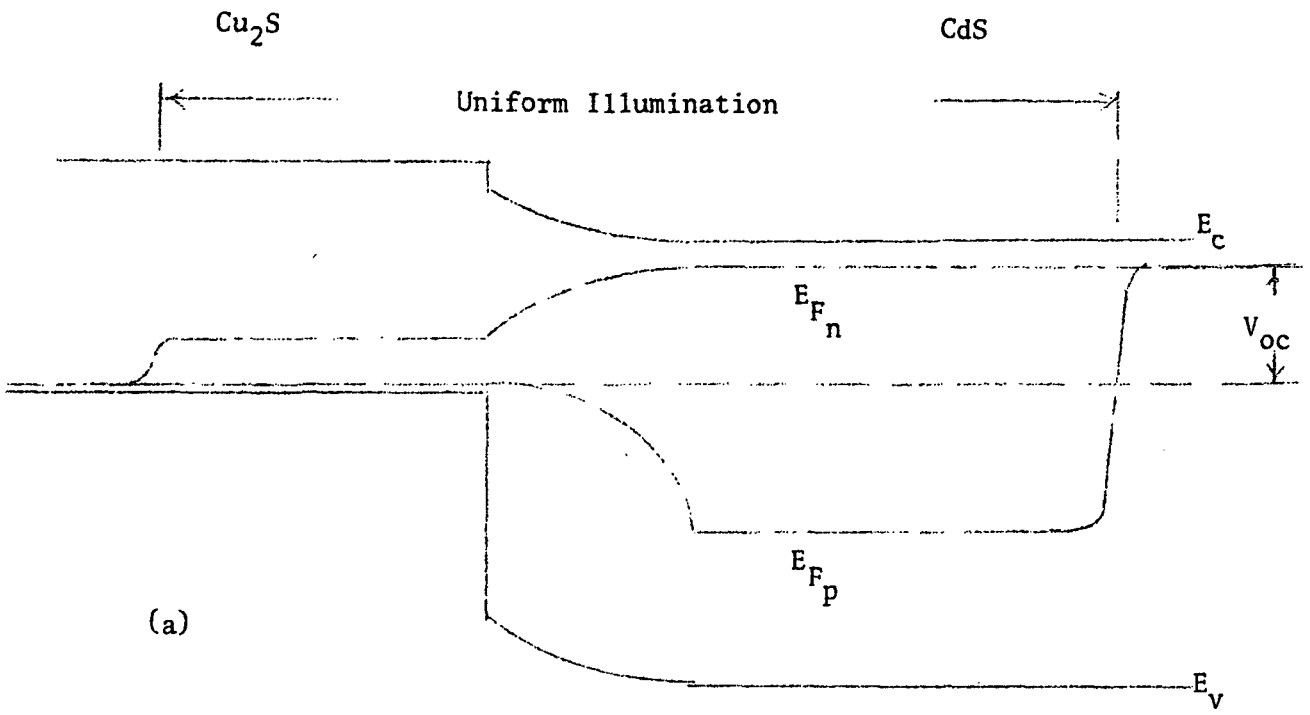

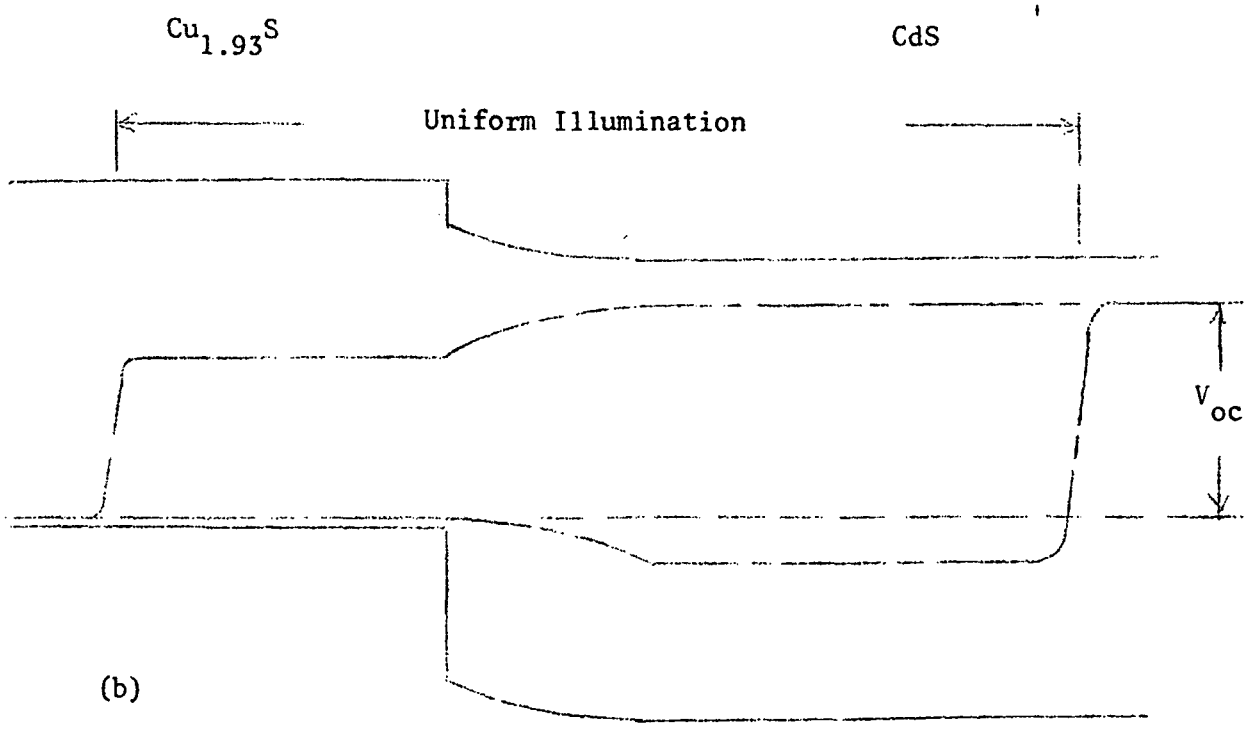

FIGURE 4.4.1: Illustration of Different V_{oc} Expected for Cu_2S:CdS (a) and $Cu_{1.93}S$:CdS (b) Photovoltaic Cells.

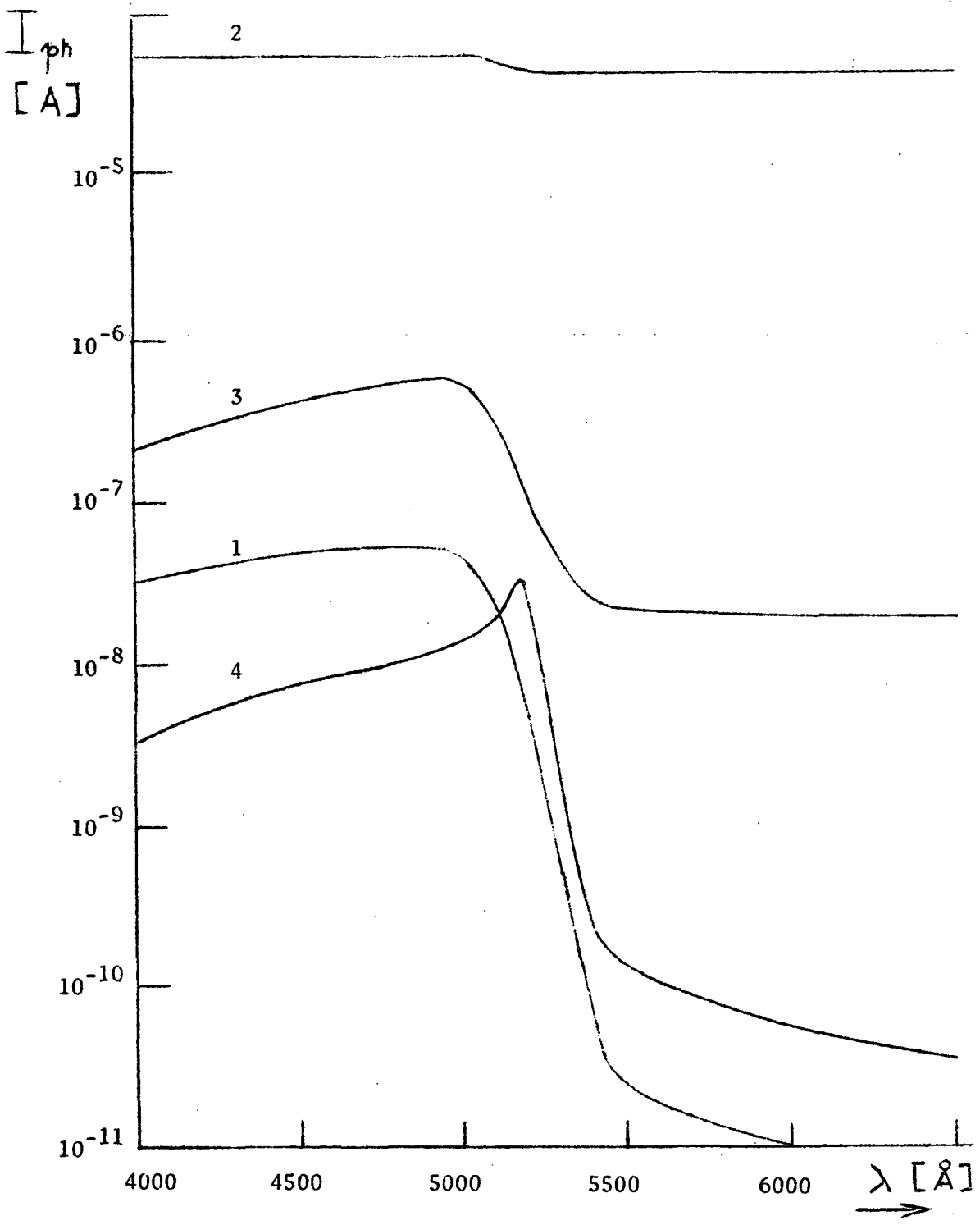

Curve 1: Untreated crystal. Atmospheric pressure.

Curve 2: After 225° C Heat Treatment.

Curve 3: After 380° C Heat Treatment.

Curve 4: After 400° C Heat Treatment.

FIGURE 4.5.1: SDP of CdS Crystal 861-1 at RT

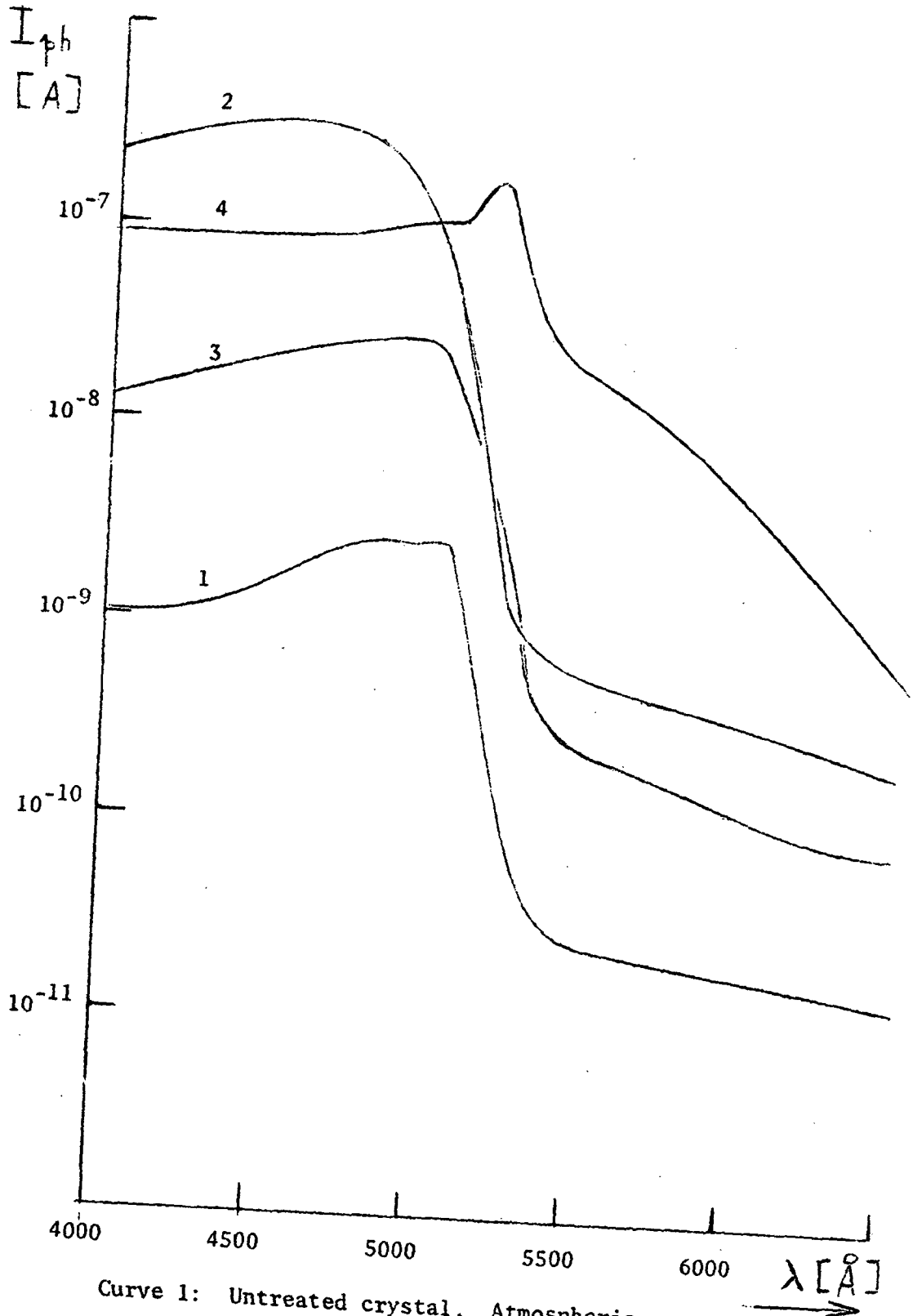

Curve 1: Untreated crystal. Atmospheric pressure.
Curve 2: After 100° C Heat Treatment.
Curve 3: After 180° C Heat Treatment.
Curve 4: After 210° C Heat Treatment.

FIGURE 4.5.2: SDP of CdS Crystal 861-2 at RT

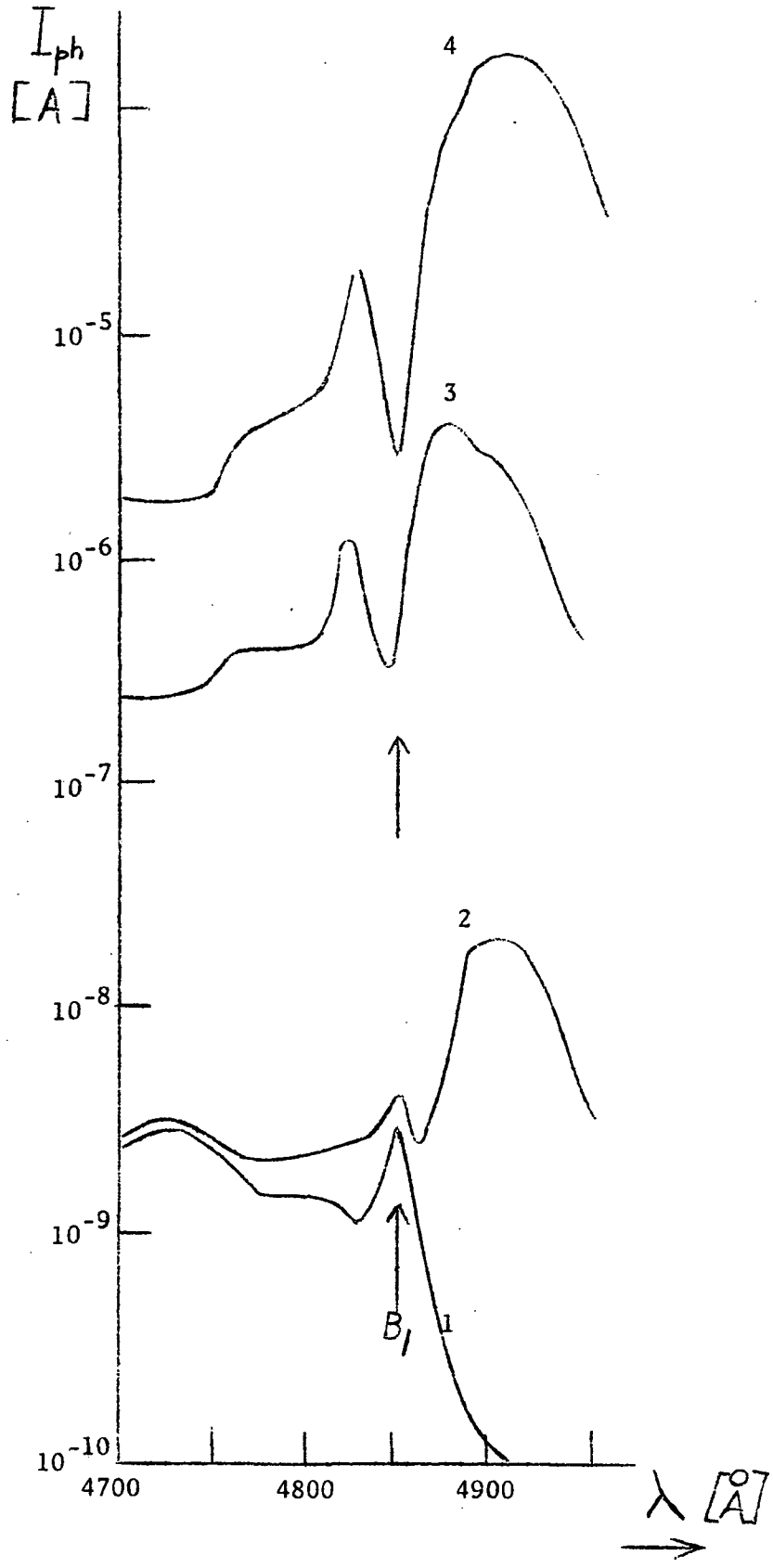

FIGURE 4.5.3: SDP of CdS Crystal 861-2 at LNT

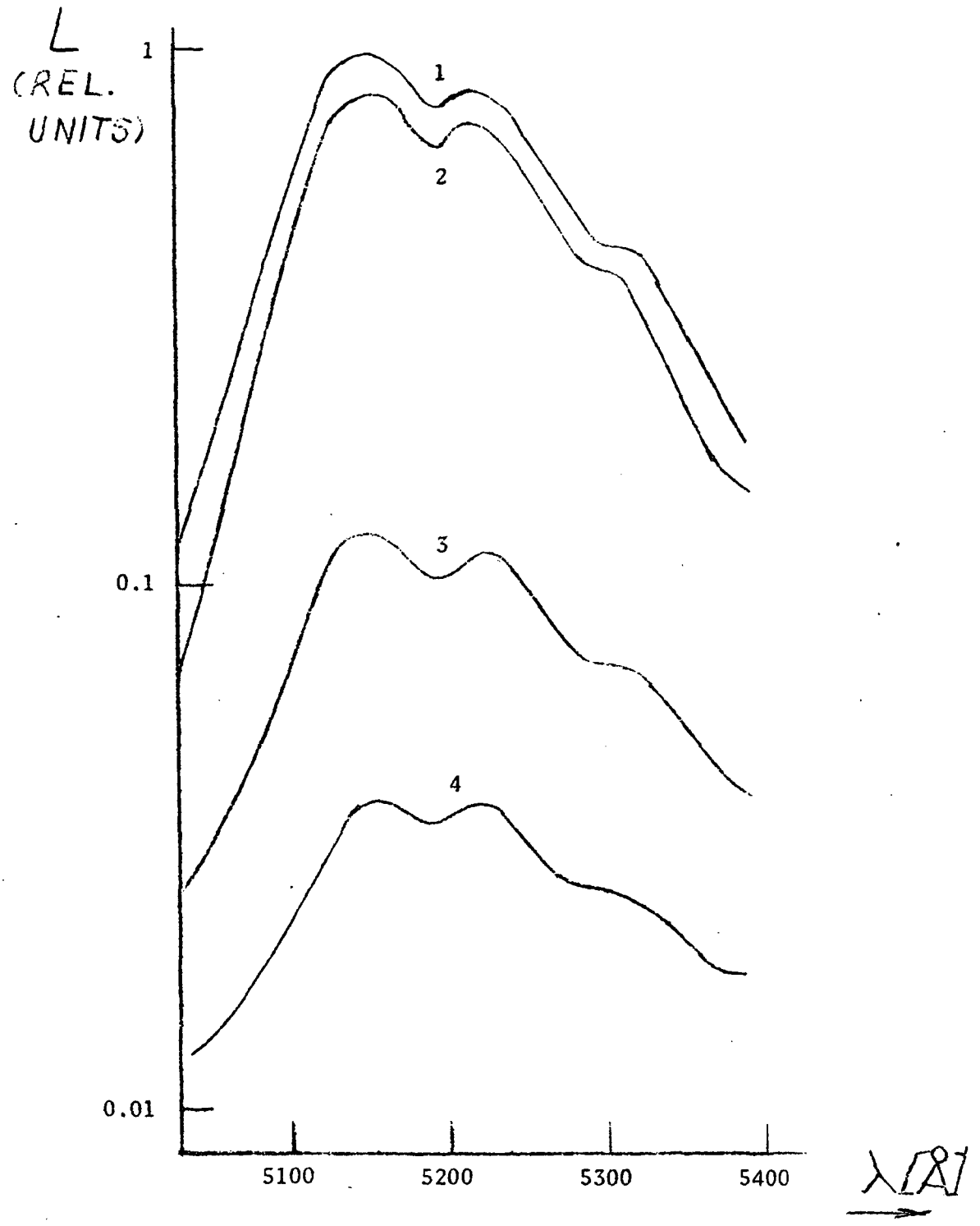

1. Before treatment
2. After 240° C treatment
3. After 2nd 240° C treatment
4. After 270° C treatment

$E \perp c$

FIGURE 4.5.4: Green-edge Luminescence of CdS Crystal 861-2 at LNT

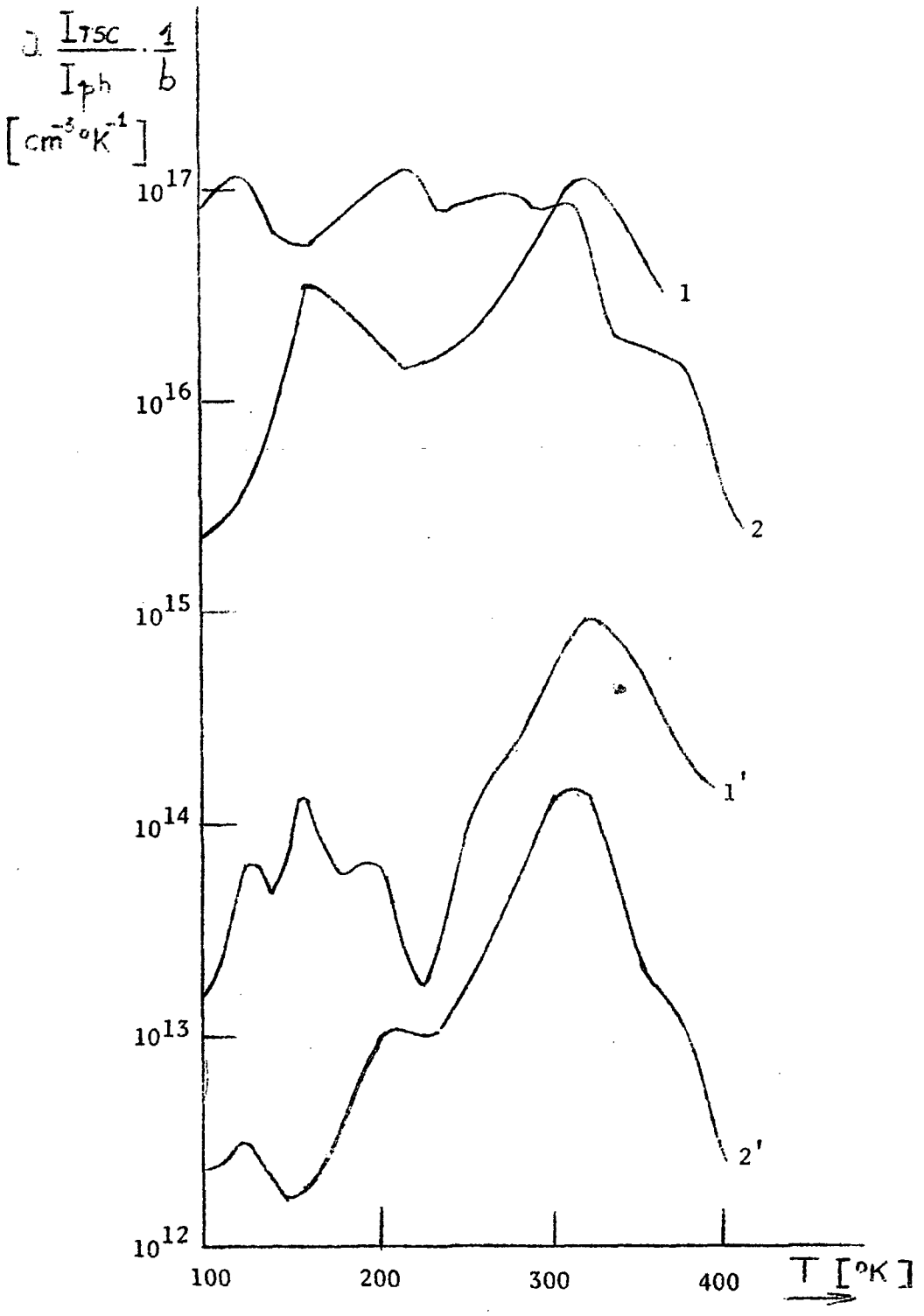

Curve 1: Class I State. Intrinsic excitation.
Curve 2: Class II State. Intrinsic excitation.
Curve 1': Class I State. Extrinsic excitation.
Curve 2': Class II State. Extrinsic excitation.

FIGURE 4.5.5: Normalized TSC Curves for Crystal 861-2

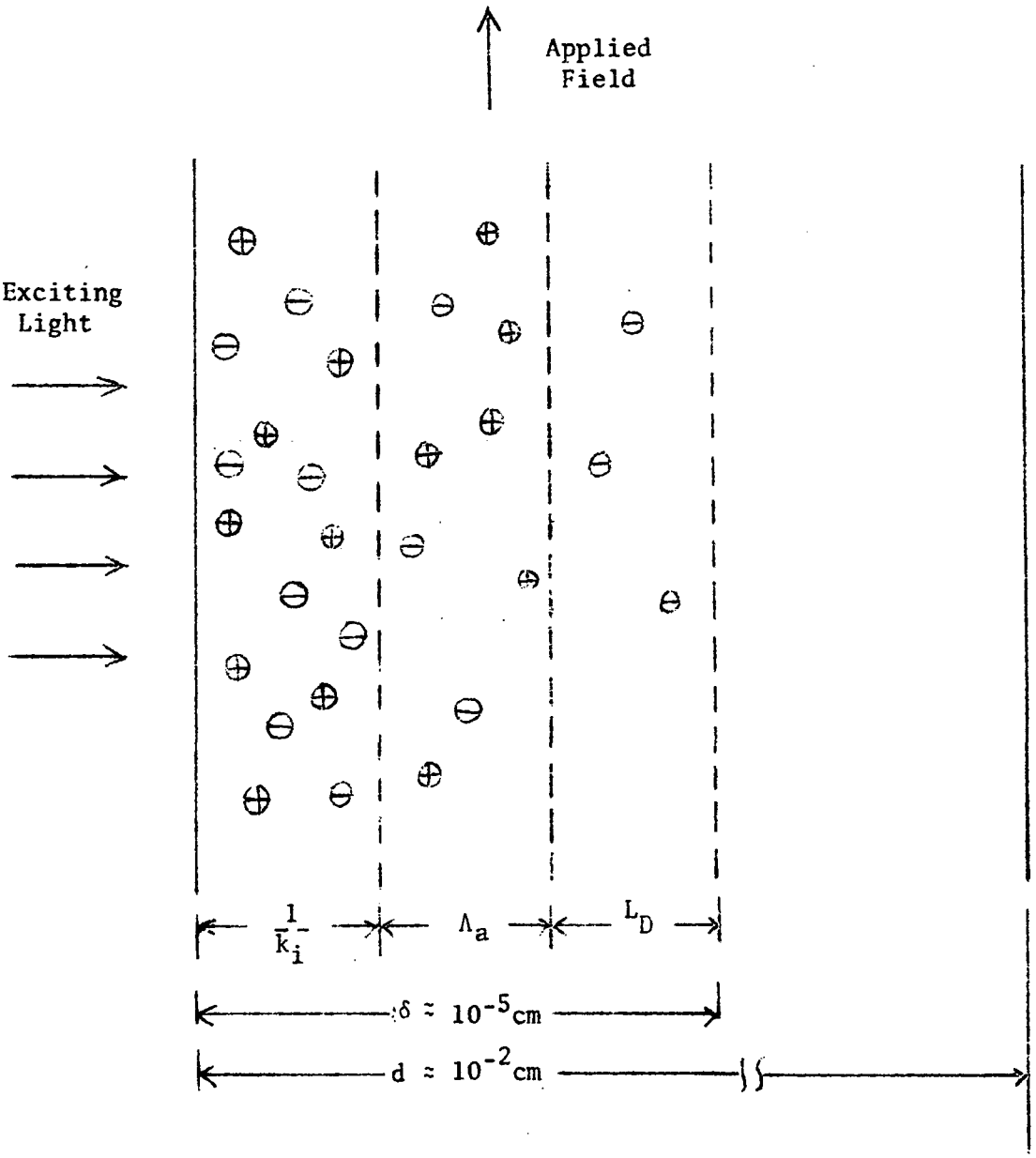

FIGURE 4.5.6:

Photoconductivity under intrinsic excitation in a CdS crystal of width $d \approx 10^{-2}$ cm. The applied field and thus the current density, are directed along the c-axis. The exciting light is at right angles to them.

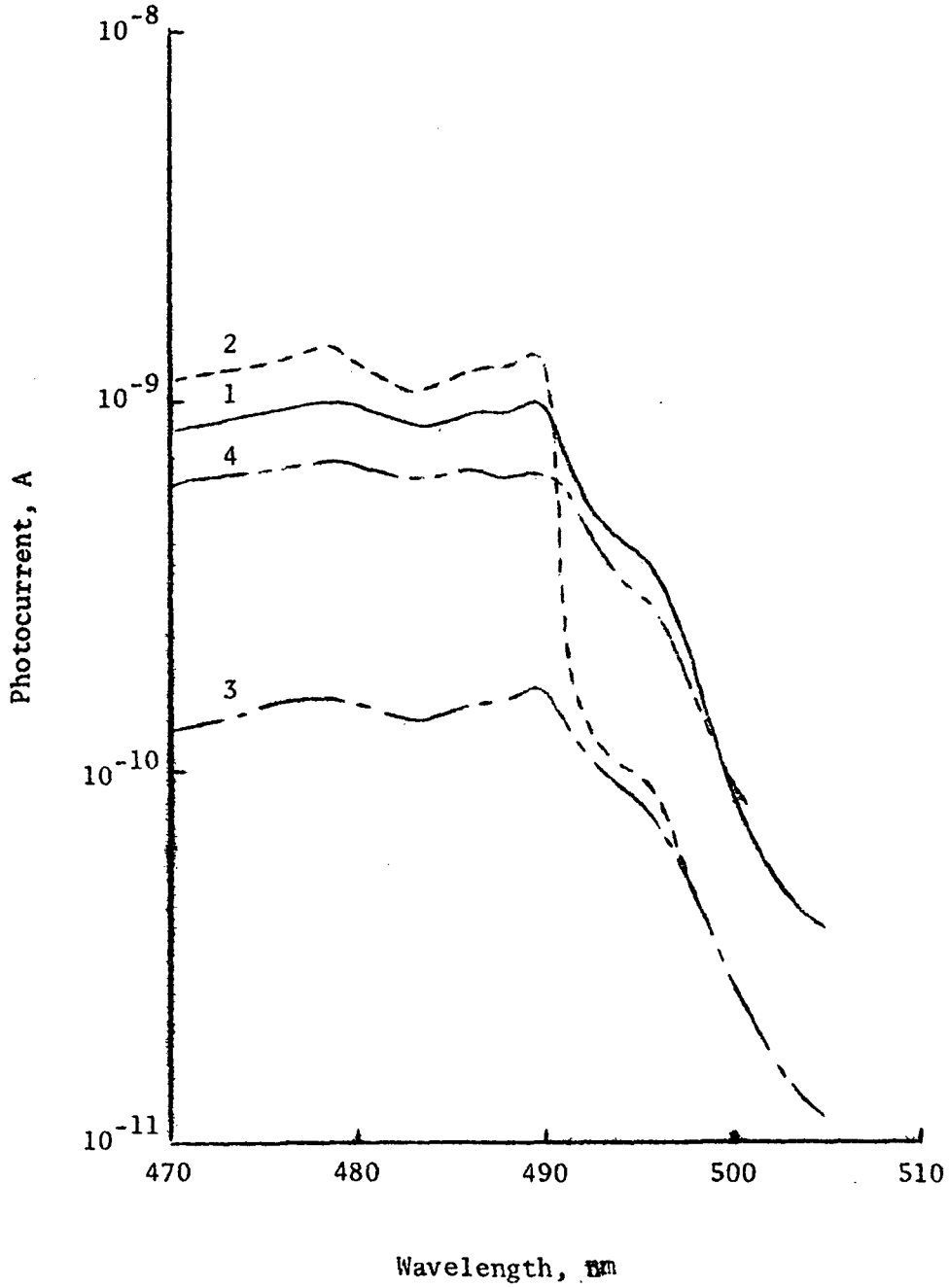

FIGURE 4.6.1:

SDP at LNT, E $\perp$ c 1) Before irradiation, 2) Immediately after irradiation, 3) Second scan immediately after irradiation, and 4) Several days after irradiation.

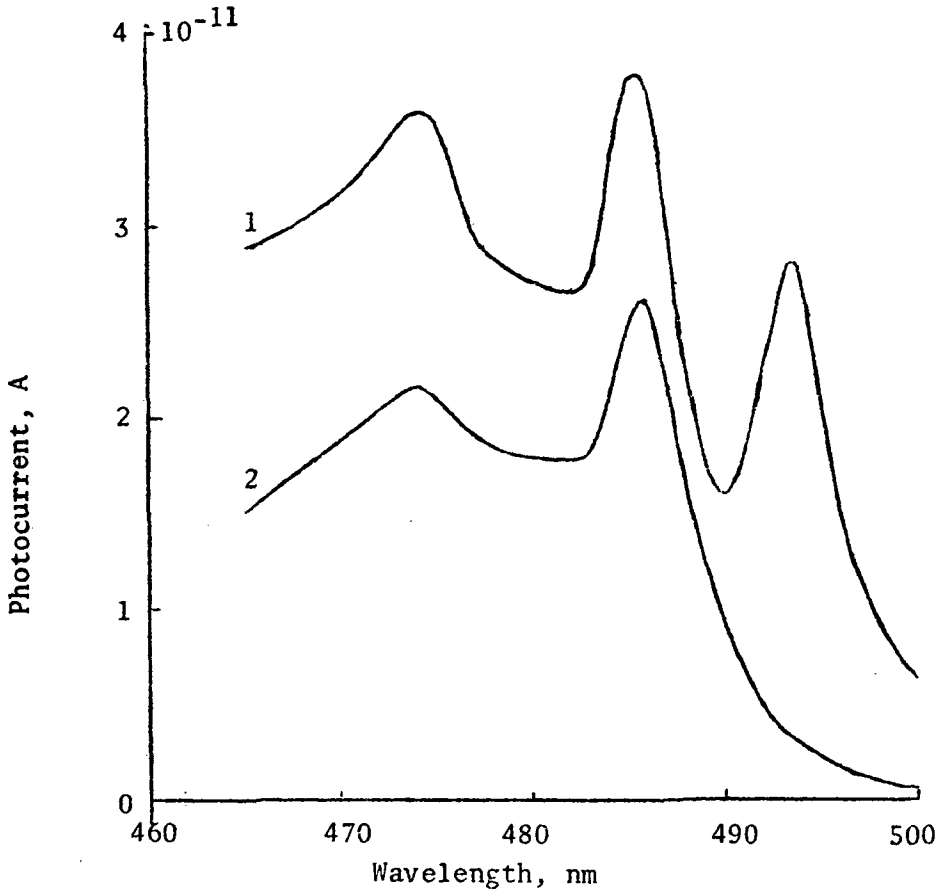

FIGURE 4.6.2: SDP at LNT for E||c: 1) No IR illumination, 2) With IR illumination.

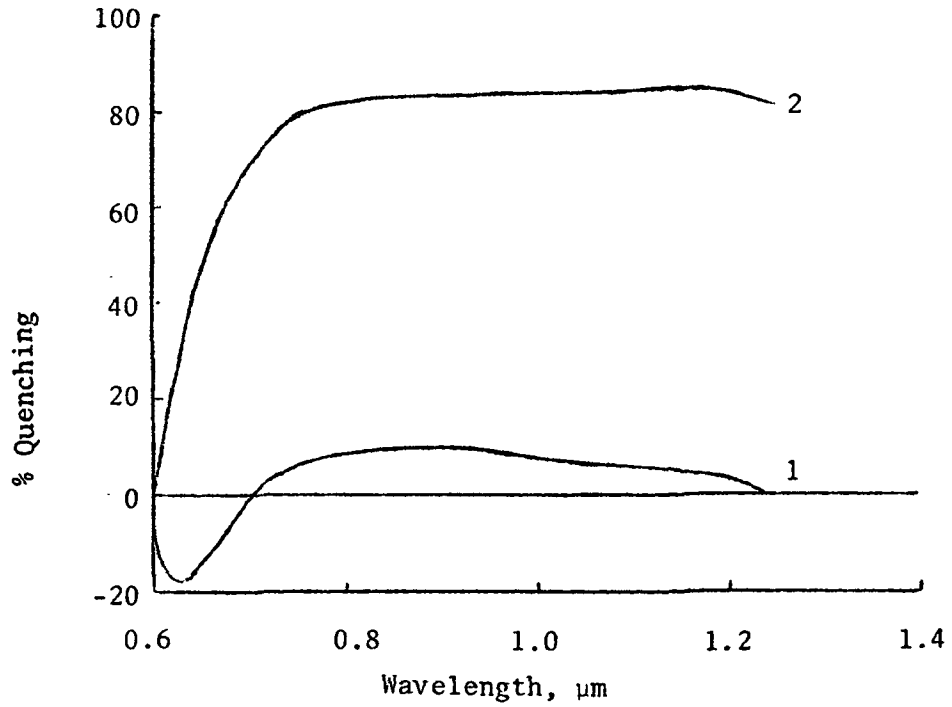

FIGURE 4.6.3: IR Quenching of Photocurrent for the 1) B exciton, and 2) Bound exciton.

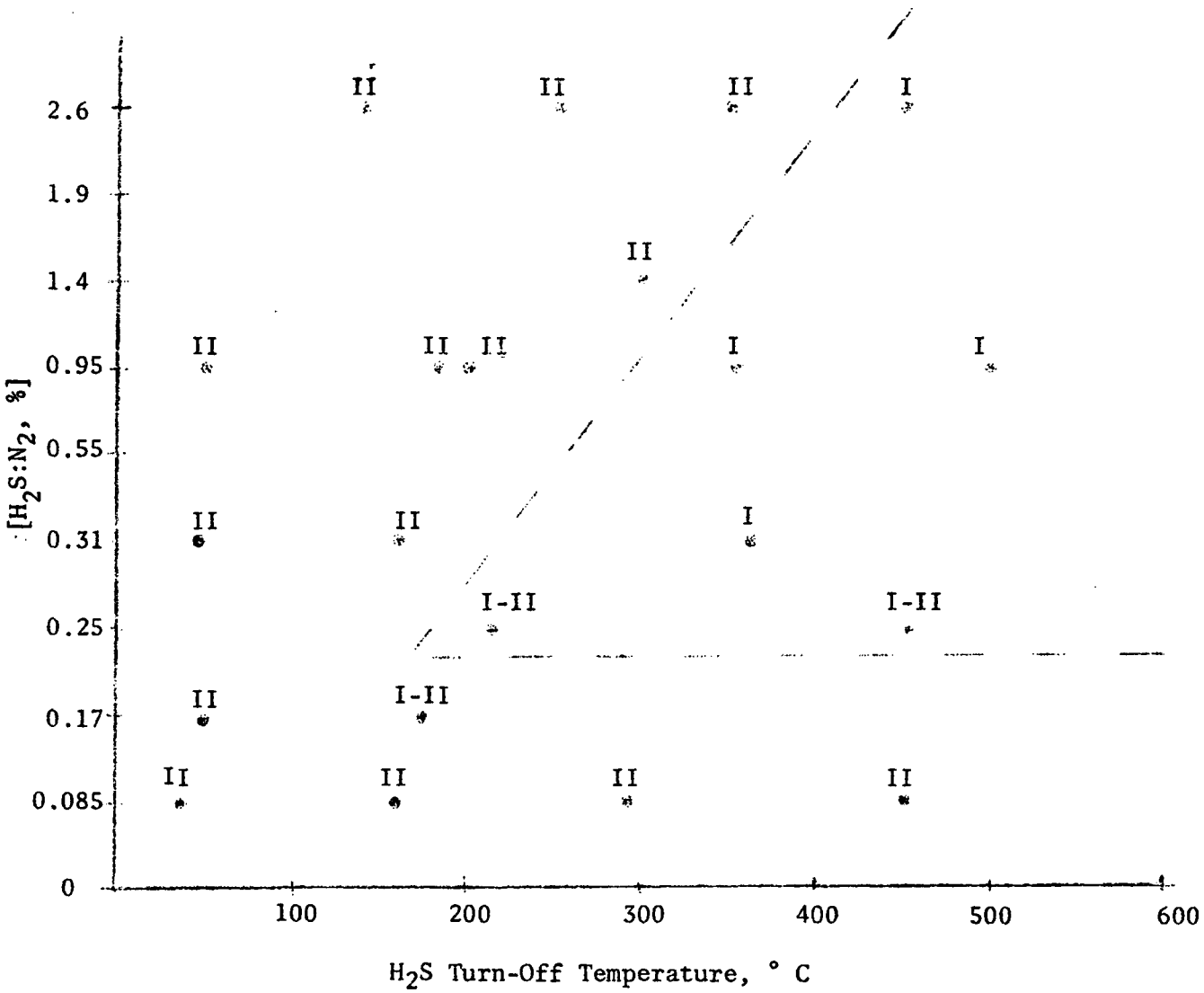

FIGURE 4.7.1: Dependence of Class of CdS Crystals on H_2S Concentration and H_2S Turn-Off Temperature